

---

# SCALING LARGE LANGUAGE MODELS FOR NEXT-GENERATION SINGLE-CELL ANALYSIS

---

**Syed Asad Rizvi\***,<sup>†</sup>  
Yale University, Google Research

**Daniel Levine\***  
Yale University

**Aakash Patel\***  
Yale University

**Shiyang Zhang\***  
Yale University

**Eric Wang\***  
Google DeepMind

**Curtis Jamison Perry\***  
Yale University

**Nicole Mayerli Constante**  
Yale University

**Sizhuang He**  
Yale University      **David Zhang**  
Yale University      **Cerise Tang**  
Yale University      **Zhuoyang Lyu**  
Brown University      **Rayyan Darji**  
Yale University      **Chang Li**  
Yale University

**Emily Sun**  
Yale University      **David Jeong**  
Yale University      **Lawrence Zhao**  
Yale University      **Jennifer Kwan**  
Yale University      **David Braun**  
Yale University      **Brian Hafler**  
Yale University

**Hattie Chung**  
Yale University      **Rahul M. Dhodapkar**  
University of Southern California

**Bryan Perozzi**  
Google Research      **Jeffrey Ishizuka<sup>‡</sup>**  
Yale University  
jeffrey.ishizuka@yale.edu      **Shekoofeh Azizi<sup>‡</sup>**  
Google DeepMind  
shekazizi@google.com      **David van Dijk<sup>‡</sup>**  
Yale University  
david.vandijk@yale.edu

October 10, 2025

## ABSTRACT

Single-cell RNA sequencing has transformed our understanding of cellular diversity, yet current single-cell foundation models (scFMs) remain limited in their scalability, flexibility across diverse tasks, and ability to natively integrate textual information. In this work, we build upon the Cell2Sentence (C2S) framework, which represents scRNA-seq profiles as textual “cell sentences,” to train Large Language Models (LLMs) on a corpus comprising over one billion tokens of transcriptomic data, biological text, and metadata. Scaling the model to 27 billion parameters yields consistent improvements in predictive and generative capabilities and supports advanced downstream tasks that require synthesis of information across multi-cellular contexts. Targeted fine-tuning with modern reinforcement learning techniques produces strong performance in perturbation response prediction, natural language interpretation, and complex biological reasoning. This predictive strength directly enabled a dual-context virtual screen that uncovered a striking context split for the kinase inhibitor silmitasertib (CX-4945), suggesting its potential as a synergistic, interferon-conditional amplifier of antigen presentation. Experimental validation in human cell models unseen during training confirmed this hypothesis, demonstrating that C2S-Scale can generate biologically grounded, testable discoveries of context-conditioned biology. C2S-Scale unifies transcriptomic and textual data at unprecedented scales, surpassing both specialized single-cell models and general-purpose LLMs to provide a platform for next-generation single-cell analysis and the development of “virtual cells.”

---

\* = Equal contribution

† = Work partially done during internship at Google Research

‡ = Corresponding author

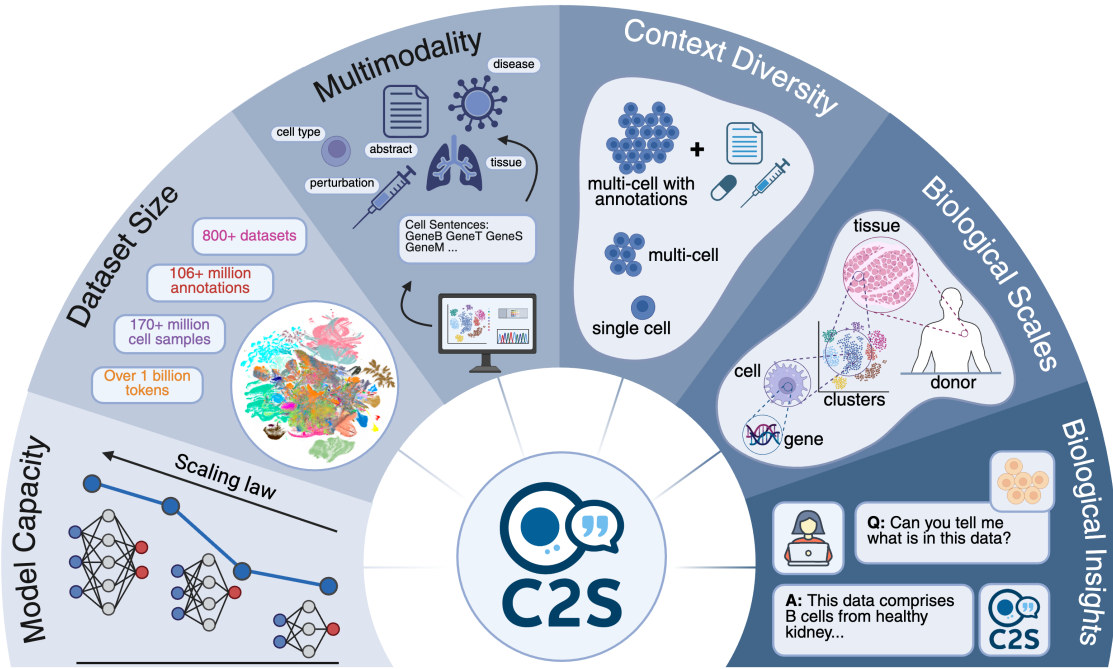


Figure 1: Scaling LLM-based single-cell analysis. A multidimensional expansion of the C2S [14] framework, demonstrating advances in model capacity, dataset size, multimodality, multi-cell support, and integration across biological scales, from single cells to organism-wide insights in natural language. This framework bridges computational innovation with biological discovery, accelerating next-generation single-cell analysis.

## 18 1 Introduction

19 Single-cell RNA sequencing (scRNA-seq) has revolutionized our understanding of cellular heterogeneity by enabling  
20 the profiling of gene expression at single-cell resolution [1]. This technology has generated massive data atlases such  
21 as CELLxGENE [2] and the Human Cell Atlas [3], offering unparalleled opportunities for computational methods  
22 to extract biological insights from this data. Recent transcriptomic foundation models (FMs), such as scGPT [4],  
23 Geneformer [5], scFoundation [6], and scGenePT [7] have shown promise in modeling single-cell transcriptomic data at  
24 scale. Despite these advances, current models are often limited by custom architectures constrained to scRNA-seq data,  
25 hindering their scalability to larger model sizes, integration of different data modalities, and ability to perform diverse  
26 generative and predictive tasks. These limitations restrict the ability of expression-only foundation models to synthesize  
27 insights across datasets, modalities, and biological contexts, and highlight the opportunity for new approaches that can  
28 integrate diverse data types, including the rich contextual information contained in biological text and metadata.

29 Large Language Models (LLMs) [8, 9, 10] offer a promising solution to these challenges. Widely used in natural  
30 language processing (NLP), LLMs exhibit consistent performance improvements with scale across diverse downstream  
31 tasks [11, 12]. Their ability to process vast text corpora and generalize effectively to new applications makes them  
32 well-suited for addressing the limitations of current expression-only models. Cell2Sentence (C2S) [13, 14] provides a  
33 framework to leverage LLMs for biology by transforming high-dimensional single-cell data into a textual format. By  
34 converting scRNA-seq profiles into “cell sentences” – sequences of gene names ordered by expression level – C2S  
35 positions single-cell data within the LLM framework, providing better scalability and infrastructure advantages than  
36 specialized model architectures. This data transformation strategy simplifies model development and deployment, and  
37 enables easy integration of transcriptomic data with diverse modalities, including metadata, experimental conditions,  
38 and textual descriptions from biological publications.

39 Here, we introduce **C2S-Scale**, a new family of LLMs trained on a multimodal corpus of over 50 million cells and  
40 associated text. We show that scaling these models up to 27 billion parameters leads to consistent performance  
41 improvements across a range of predictive and generative tasks (Fig. 1). C2S-Scale’s flexible context allows it to analyze  
42 cellular interactions and diverse biological information in multi-cell contexts, enabling sophisticated applications from  
43 predicting perturbation responses to answering complex biological questions. To further enhance the biological accuracy  
44 of model outputs, we developed refinement techniques with reinforcement learning (GRPO) to align model predictions

- 45 with key biological objectives. We also introduce a novel metric, single-cell Fréchet Inception Distance (scFID), for  
46 assessing generative performance.
- 47 To demonstrate this platform's capacity for novel biological discovery, we programmed a dual-context virtual screen  
48 designed to find interferon (IFN)-conditional amplifiers of antigen presentation. The screen revealed a pronounced  
49 context split for the kinase inhibitor silmitasertib, which has not been reported to enhance MHC-I expression. Our  
50 model predicted a strong effect in the context of low levels of IFN exposure, but no effect in the absence of IFN  
51 signaling. We validated this prediction in targeted wet lab experiments using neuroendocrine human cell models not  
52 seen during training.
- 53 By releasing our models and resources, we provide a powerful, open-source platform for next-generation single-cell  
54 analysis.

## 55 2 Results

### 56 2.1 C2S-Scale: A foundation model for single-cell analysis at scale

- 57 To create a model capable of jointly interpreting transcriptomic data and biological text, we developed **C2S-Scale**, a  
58 family of LLMs trained on a large-scale corpus of scRNA-seq data and associated text (Fig. 2). C2S-Scale builds on the  
59 Cell2Sentence framework [13, 14], which represents single-cell gene expression profiles as textual “cell sentences”:  
60 lists of gene names ranked by their expression level (Fig. 2B). This representation preserves relative gene expression  
61 while also allowing the model to leverage its knowledge about genes learned from vast text corpora. The transformation  
62 from expression to cell sentence representation is reversible with minimal information loss due to the strong relationship  
63 between relative position and original gene expression [13, 14] (examples provided in Fig. 10).
- 64 Training C2S-Scale consists of two phases: a self-supervised general pretraining phase on our large-scale corpus,  
65 followed by additional tuning for specific tasks. To assemble the pretraining corpus, we collected over 50 million  
66 human and mouse transcriptomes from a diverse range of tissues gathered from the CELLxGENE [2] and Human Cell  
67 Atlas [3] data atlases, along with associated annotations, papers, and metadata. We pretrained C2S-Scale on a variety of  
68 tasks constructed using samples from the raw corpus, encompassing predictive and generative tasks on both single and  
69 multi-cell context (Table 1). This allows the LLM to learn to model cell sentences while simultaneously learning to  
70 follow prompt instructions for common scRNA-seq analysis tasks. During the fine-tuning phase, the pretrained model  
71 is specialized for a particular task on a new dataset.

### 72 2.2 C2S-Scale demonstrates broad predictive and generative capabilities

- 73 We evaluated C2S-Scale on a diverse spectrum of single-cell tasks, outperforming or matching existing state-of-the-art  
74 transcriptomic and natural language foundation models (Fig. 3). For traditional single-cell analysis tasks, C2S-Scale  
75 achieved results competitive with expression-only foundation models such as scGPT [4] and Geneformer [5] on immune  
76 [15] and lung [16] datasets. For example, on a diverse immune tissue dataset, C2S-Scale predicted cell type annotations  
77 in natural language with 95.43% accuracy, slightly better than scGPT (93.1%) and Geneformer (94.0%). C2S-Scale  
78 models also generated rich cell embeddings when given a cell sentence as input, capturing both transcriptional and  
79 contextual information from natural language. We also construct a multimodal integration task assessing the similarity  
80 of embeddings of paired single-cell and bulk data. Notably, C2S-Scale could accurately match single-cell profiles  
81 to their corresponding bulk RNA-seq profiles despite no prior exposure to bulk RNA-seq data, suggesting that C2S  
82 captures a more biologically meaningful representation of cellular states through cell sentences.
- 83 Beyond these predictive tasks, C2S-Scale supports complex generative and interpretive functions not present in most  
84 other transcriptomic foundation models. For instance, C2S-Scale accurately predicts cellular transcriptional responses  
85 to perturbations, even generalizing to combinatorial and previously unseen conditions (described further in Section 2.7).  
86 Furthermore, when tasked with interpreting scRNA-seq data using natural language, C2S-Scale outperformed even  
87 leading general-purpose LLMs such as Llama [17, 18], GPT-4o [19] and Gemini [20] at tasks such as generating  
88 descriptive captions for cell clusters and summarizing entire datasets. Remarkably, C2S-Scale generalizes effectively  
89 to completely unseen scRNA-seq studies (Fig. 3), demonstrating its interpretive capabilities on completely unseen  
90 datasets. On question answering in natural language, C2S-Scale outperformed the best public LLM model (GPT-4o) by  
91 3% in BERTScore, highlighting its answer quality and natural language capabilities. The ability to generate biologically  
92 meaningful insights in natural language makes C2S-Scale a uniquely powerful and accessible tool for interacting  
93 with and interpreting single-cell data. Detailed description of each task and evaluation methodology can be found in  
94 Section 4.

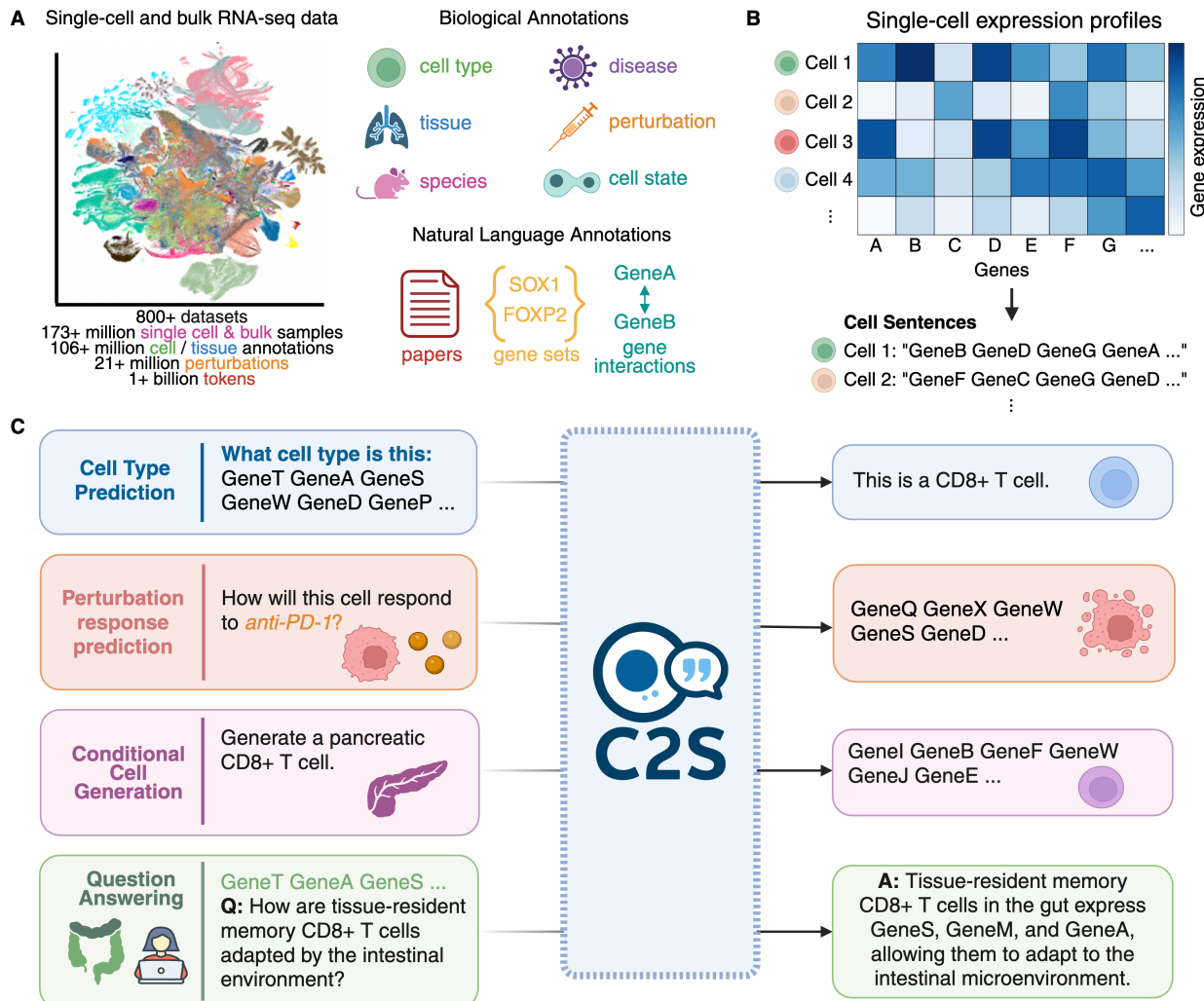


Figure 2: C2S-Scale bridges scRNA-seq data and natural language by training LLMs to perform single-cell analysis tasks on diverse, multimodal data. (A) A multimodal corpus of over 50 million human and mouse transcriptomes is gathered from public data atlases, encompassing cellular expression from a diverse range of tissues, textual annotations, papers, gene sets, and disease labels from scRNA-seq studies. (B) C2S rank-orders genes by expression and converts them to natural language “cell sentences”, leveraging powerful LLM architectures without the need for custom modifications. (C) C2S supports diverse downstream use cases, including perturbation prediction, generative tasks, and advanced biological reasoning tasks such as question answering.

95 Taken together, these results show that C2S-Scale is a uniquely versatile tool. It is the only model to our knowledge  
 96 capable of spanning this entire range of single-cell analysis tasks, including prediction, generation, and natural language  
 97 reasoning. This positions C2S-Scale as a comprehensive platform for next-generation biological discovery.

### 98 2.3 Scaling enhances the biological reasoning capabilities of C2S-Scale

99 A central principle of modern LLMs is that their performance improves predictably with increased scale [11, 12]. We  
 100 analyzed the performance of C2S-Scale at a range of model capacities to test whether similar effects exist for LLMs in  
 101 single-cell analysis. Our results show that similar scaling laws emerge when LLMs are trained on natural language  
 102 representations of transcriptomic data: as model size increased from 410 million to 27 billion parameters, we observed  
 103 consistent performance improvements across diverse biological tasks, including cell type annotation, tissue inference,  
 104 and conditional cell generation (Fig. 4C).

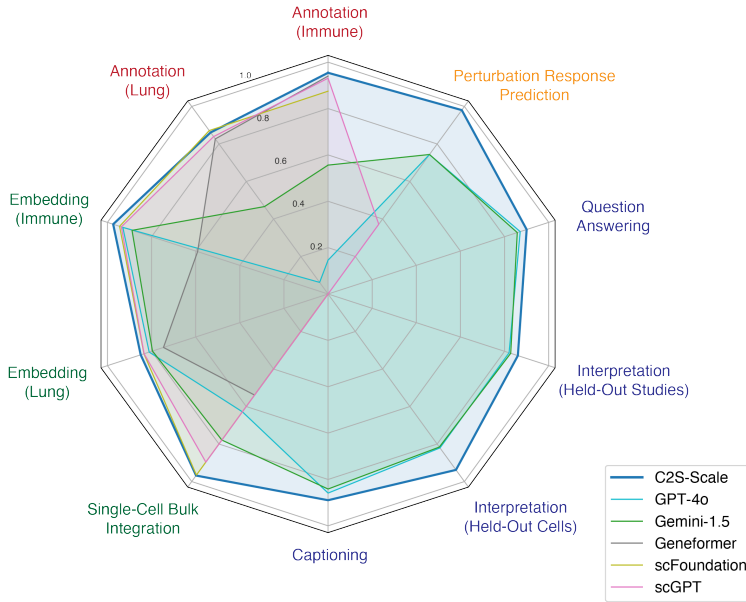


Figure 3: C2S-Scale outperforms both transcriptomic and natural language foundation models across diverse predictive and generative single-cell tasks. Tasks include standard single-cell analysis tasks such as cell type annotation (red) and cell embedding (green), a generative perturbation response prediction task (orange), and natural language interpretation tasks including cluster captioning, dataset interpretation, and question answering tasks (blue). Raw performance numbers are available in the Supplement. C2S-Scale is the only model capable of spanning the entire range of single-cell analysis tasks, and demonstrates competitive performance on all tasks.

105 These scaling trends were consistent in both fully fine-tuned and parameter-efficient training regimes where only a  
106 fraction of model parameters were trained (Fig. 4D). Furthermore, for a fixed model size, performance also scaled with  
107 the amount of training data seen by the model (Fig. 4E). Together, these results establish that increasing both model and  
108 dataset size is a reliable strategy for enhancing the biological reasoning capabilities of cellular language models. This  
109 suggests that the full potential of this approach has not yet been reached and that future, larger models may yield even  
110 greater biological insights.

#### 111 2.4 Interpreting single-cell data across biological scales using natural language

112 Natural language interpretation is an underexplored aspect of single-cell analysis, enabling researchers to bridge  
113 experimental scRNA-seq data with existing biological literature and providing a user-friendly tool for biologists to  
114 interact with and interpret their data. Existing LLM-based single-cell models such as GenePT [21] and scGenePT [7]  
115 offered limited integration of natural language and single-cell data, focusing primarily on using language embeddings  
116 in single-cell architectures and tasks. C2S-Scale bridges large-scale training on transcriptomic data with the natural  
117 language pretraining and generative capabilities of LLMs, enabling natural language interpretation of scRNA-seq data  
118 at multiple scales of biology, illustrated in Fig. 5A.

119 We benchmark C2S-Scale on a series of natural language interpretation tasks at various scales of biology, evaluating  
120 its ability to reason about and generate meaningful descriptions about data. At the **individual cell level**, C2S-Scale is  
121 able to accurately annotate cell types in natural language given cell sentences as input. The model is first fine-tuned  
122 on a diverse immune tissue dataset [15] to predict cell type labels in natural language. C2S-Scale is able to correctly  
123 classify almost all cell types on a held-out partition of the immune tissue data (Fig. 5B), demonstrating C2S-Scale's  
124 effectiveness at standard single-cell analyses.

125 At the **cluster level**, we introduce a novel task called Cluster Captioning, where the goal is to generate biologically  
126 meaningful descriptions for groups of cells from the same tissue and batch within a scRNA-seq dataset. To create  
127 training data for this task, we use GPT-4o [19] to generate natural language captions for cell clusters derived from  
128 annotated datasets (Methods Section 4.6). C2S-Scale is fine-tuned to predict these captions given multiple input cell  
129 sentences from each cluster and is evaluated on held-out clusters not seen during training. Performance is measured  
130 using BioBERTScore [22], which quantifies semantic similarity between generated and ground-truth captions. As

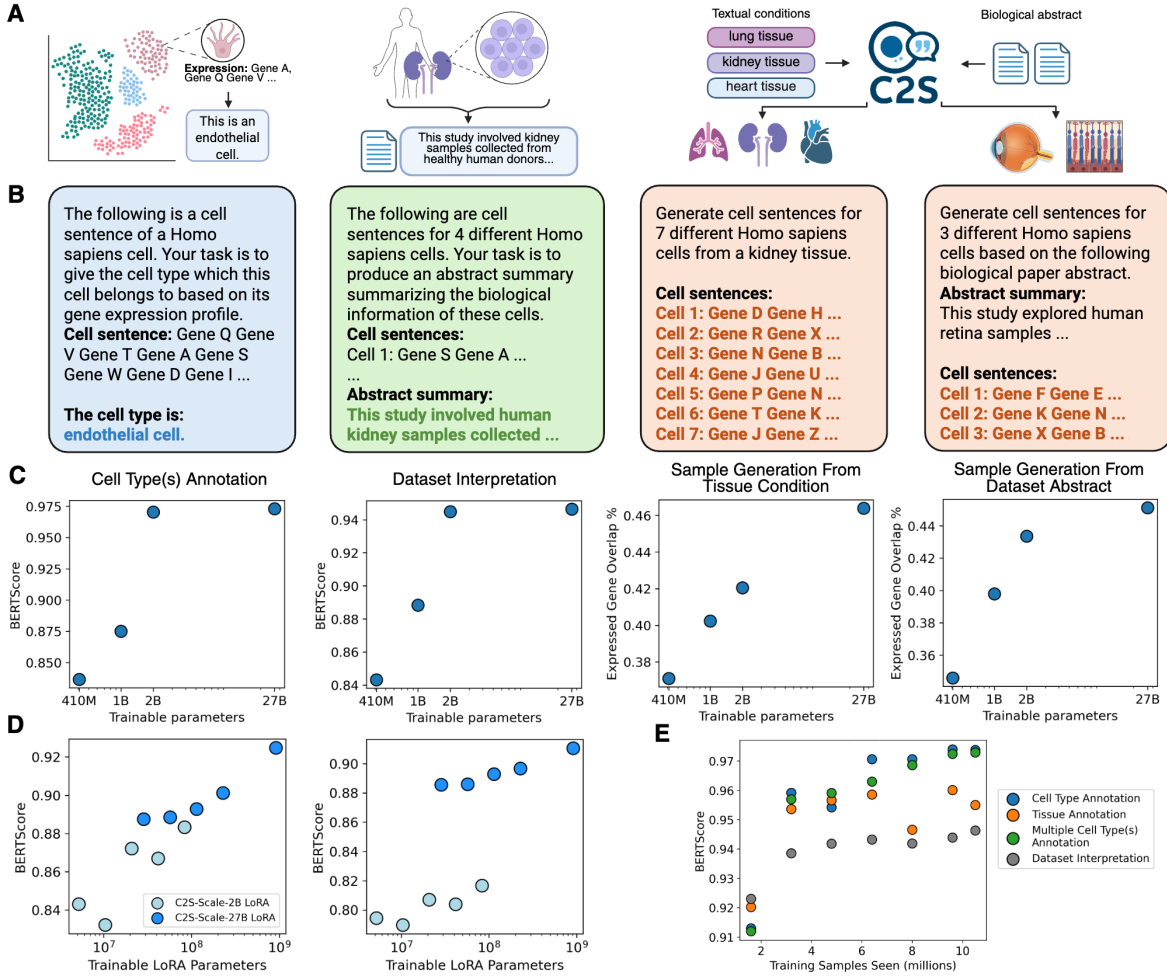
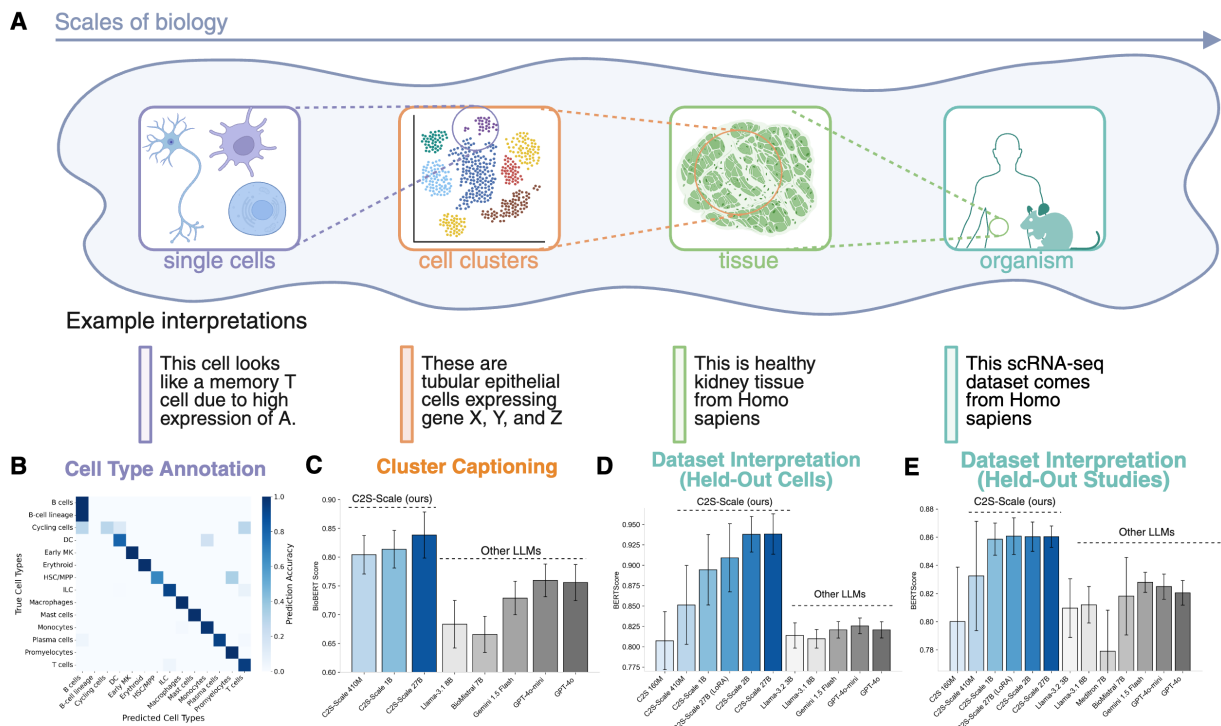


Figure 4: Cell2Sentence demonstrates consistent scaling in performance with increasing model capacity across diverse single-cell analysis tasks. (A) Examples of predictive and generative tasks on single-cell data. (B) Natural language prompts and responses for tasks in (A), colored by expression generation (red), predictive (blue), and language generation (green) tasks. (C) Performance scaling of fully fine-tuned C2S models on cell type annotation, dataset interpretation, and conditional sample generation tasks. (D) LoRA fine-tuned C2S-Scale-2B and 27B models demonstrate performance scaling with increased model capacity in the parameter-efficient regime. (E) Performance scaling by number of training samples seen by C2S-Scale-27B.



**Figure 5:** C2S-Scale enables natural language interpretation of scRNA-seq data at multiple scales, from single cells to entire datasets. (A) Different scales of biological data interpretation, from single cells to organism and dataset-level annotation. (B) Ground truth and predicted cell types for immune cells extracted from 16 different tissues of adult human donors [15], demonstrating the ability of C2S-Scale to annotate data at the single-cell level. (C) Cluster captioning performance on unseen scRNA-seq data clusters. Models are given multi-cell context from unseen data clusters and tasked with captioning the data, measured by BERTScore. (D-E) Performance of C2S-Scale models on natural language interpretation of entire scRNA-seq datasets on held-out cells and held-out studies. Error bars represent standard deviation across test set samples.

shown in Fig. 5C, C2S-Scale outperforms all baseline LLMs on this task, demonstrating its ability to interpret and summarize expression patterns at the cluster level.

At the **dataset level**, we further evaluate interpretive ability through a Dataset Interpretation task, where the model receives multiple cell sentences from a scRNA-seq dataset and is tasked with generating a high-level summary in the style of a biological abstract. These summaries are expected to describe key features of the dataset, including dominant cell types, tissues, disease states, or perturbations (examples provided in Fig. 11). Fig. 5D shows that C2S-Scale achieves the highest BERTScore among all evaluated models, including Llama [17, 18, 23], Meditron [24], BioMistral [25], Gemini [20], and GPT-4o [19]. Notably, C2S-Scale generalizes well to entirely unseen datasets, producing summaries that remain relevant and informative (Fig. 5E), highlighting its robust natural language understanding of scRNA-seq data.

Overall, C2S-Scale enables natural language interpretation at multiple scales, spanning single cells, clusters, and datasets. Its ability to integrate textual and biological data unlocks new opportunities for biologists to explore, annotate, and generate insights from scRNA-seq data in natural language.

## 144 2.5 C2S-Scale Learns Spatial Reasoning from Multi-cell Context and Interaction Data

145 Understanding spatial organization in tissues is fundamental to uncovering the mechanisms that govern cellular  
146 interactions, particularly in how they drive disease progression and tissue homeostasis [26, 27, 28]. Cellular niches,  
147 defined by their specific cell types, signaling molecules, and extracellular matrix components, play a crucial role in  
148 regulating these processes. Accurately predicting spatial relationships among cells from transcriptomic data alone  
149 is challenging, as traditional approaches often rely on explicitly structured spatial models or predefined interaction  
150 networks [29, 30, 31].

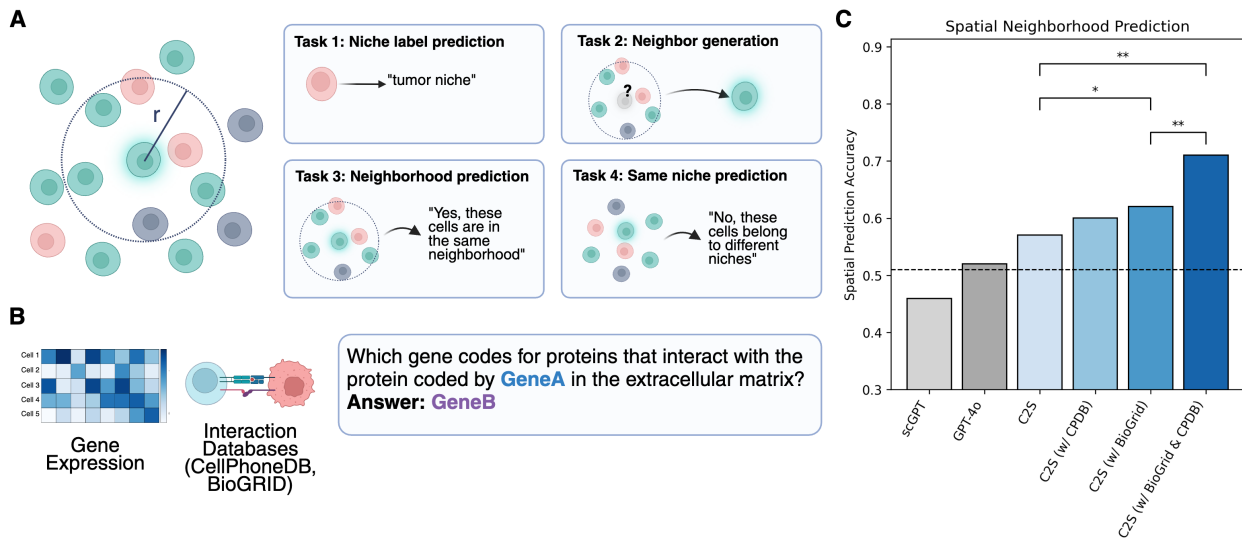


Figure 6: C2S-Scale can interpret multi-cellular spatial context and predict niche neighborhoods. (A) We fine-tune C2S-Scale on a variety of single and multi-cellular spatial tasks designed to enable C2S-Scale to perform spatial reasoning, including predicting niche labels, generating spatial neighbors, and identifying whether cells belong to the same neighborhood or niche. A “neighborhood” is defined to be cells within a fixed radius from a central cell. (B) We use publicly available gene interaction databases including BioGRID and CellPhoneDB to construct natural language interaction prompts about gene interactions. To maximize relevance, BioGRID is filtered to include only genes expressed in the CosMx dataset and restricted to extracellular proteins. (C) C2S outperforms scGPT and GPT-4o in spatial neighborhood identification accuracy. Additionally, integrating gene interactions from BioGRID and CellPhoneDB individually improves performance, and their combination provides the greatest improvement (\* =  $P < 0.05$ , \*\* =  $P < 0.01$ ; McNemar’s test). These results highlight the multi-task transfer learning potential of C2S-Scale for spatially-aware biological modeling.

- 151 Although C2S-Scale was not explicitly designed for spatial reasoning, its ability to incorporate multi-cellular context  
 152 provides a natural mechanism for modeling spatial organization. We hypothesize that by sampling and encoding cells  
 153 from shared neighborhoods, C2S-Scale can infer spatial relationships without requiring architectural modifications.  
 154 To test this, we evaluate the model’s performance in predicting spatial neighborhoods using a human liver spatial  
 155 RNA-seq dataset [32]. Additionally, we simultaneously train C2S-Scale on related tasks aimed at improving its spatial  
 156 understanding: niche label prediction, neighbor cell generation, and determining whether multiple cells belong to the  
 157 same niche (Fig. 6A). By training on these complementary tasks, C2S-Scale learns robust representations of spatial  
 158 organization, significantly outperforming both scGPT and GPT-4o in neighborhood prediction (Fig. 6C).
- 159 We further hypothesize that incorporating external biological knowledge – specifically, gene interaction networks – can  
 160 enhance spatial reasoning. Receptor-ligand and other protein-protein interactions are central to cell-cell communication,  
 161 yet many scFMs are unable to integrate this information. Instead of imposing predefined rules, we simply expose  
 162 C2S-Scale to receptor-ligand interactions from CellPhoneDB [33] and protein interaction data from BioGRID [34],  
 163 formatted as natural language prompts (Fig. 6B). This approach allows the model to implicitly integrate prior knowledge  
 164 while maintaining flexibility in how it applies this information.
- 165 Fine-tuning with gene interaction data further improves C2S-Scale’s ability to predict spatial relationships, reinforcing  
 166 the hypothesis that external molecular context enhances spatial reasoning (Fig. 6B). Notably, adding either CellPhoneDB  
 167 or BioGRID data individually improves performance, demonstrating that both receptor-ligand and protein-protein  
 168 interaction knowledge contribute to spatial reasoning (Fig. 6C). Moreover, combining both datasets results in the  
 169 greatest improvement, suggesting that integrating diverse biological interaction sources allows LLMs to develop a  
 170 richer understanding of multi-cellular organization and interactions.
- 171 A key advantage of C2S-Scale is its ability to integrate diverse data sources without requiring explicitly structured  
 172 incorporation of external knowledge. Unlike traditional methods that rely on predefined pathways or manually curated  
 173 interaction models, C2S-Scale implicitly learns to incorporate relevant information during training. This highlights a  
 174 fundamental strength of C2S: rather than designing bespoke architectures for specific tasks, we can provide relevant

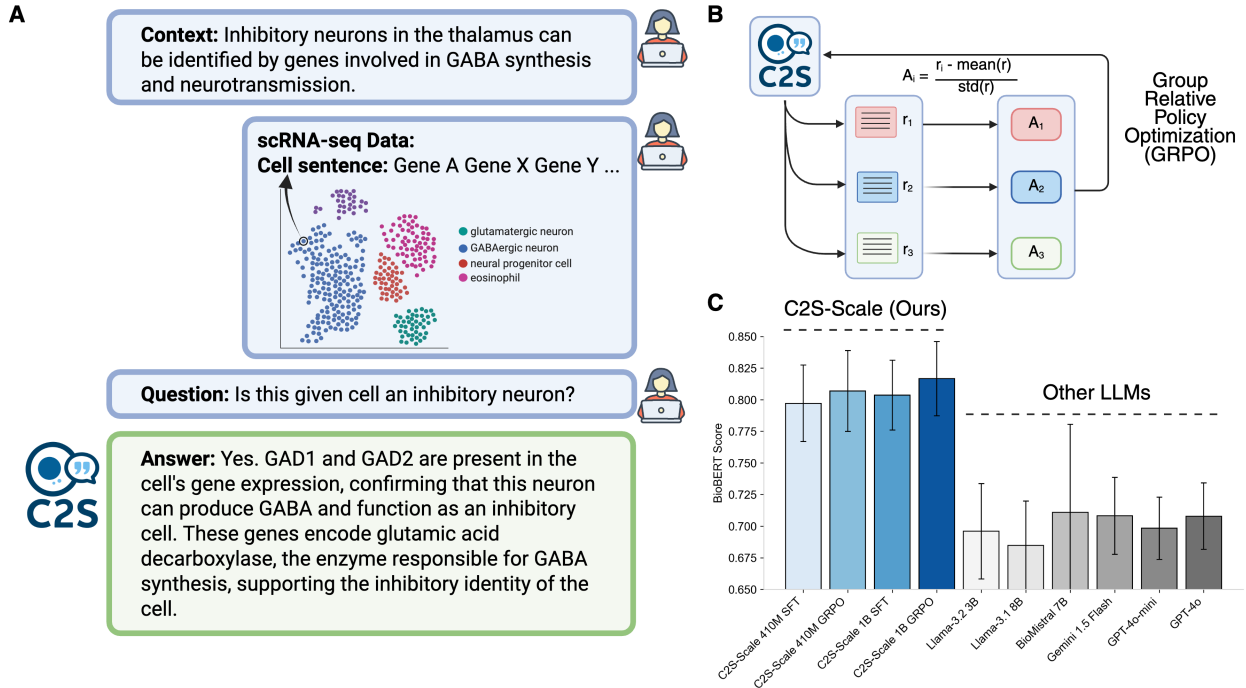


Figure 7: C2S-Scale demonstrates superior single-cell question answering performance compared to state-of-the-art (SOTA) LLMs. (A) Example QA scenario based on scRNA-seq data. (B) Overview of the GRPO framework [35], which further refines model performance by training on preference data. (C) Empirical comparison of C2S-Scale and SOTA LLMs on single-cell QA tasks, highlighting C2S-Scale's advantage in domain-specific reasoning. Error bars represent standard deviation across test set QA samples.

175 data, and the model autonomously determines how to utilize it. This capability extends beyond spatial reasoning and  
176 suggests broad applicability for integrating multimodal biological data.

## 177 2.6 Single-Cell Question Answering (QA) through Reinforcement Learning

178 QA tasks form a core part of NLP, providing a standard test to measure a model's ability to understand information and  
179 apply reasoning [36, 37, 38, 39]. In biomedical research, QA tasks are particularly valuable for assessing advanced  
180 reasoning in domain-specific contexts, as evidenced by the development of numerous specialized QA datasets for  
181 medical [40, 41] and biological [42] applications. Building on this foundation, we introduce a single-cell Question  
182 Answering (scQA) task to assess the ability of foundation models to reason about and interpret single-cell transcriptomic  
183 data.

184 The scQA dataset consists of two thousand question-answer pairs, each containing: (i) an associated biological context,  
185 (ii) relevant scRNA-seq data sampled from clusters or cell type annotations, (iii) a main question, and (iv) a final answer.  
186 Additionally, each answer is annotated with keywords to help evaluate response quality. To construct the dataset,  
187 we sample cells from scRNA-seq datasets, provide the sampled data along with associated biological manuscripts to  
188 GPT-4.5 [19], and prompt it to generate meaningful questions (Fig. 7A).

189 After supervised fine-tuning (SFT), C2S-Scale surpasses the performance of state-of-the-art LLMs on scQA (Fig. 7C),  
190 demonstrating the advantages of specialized training on transcriptomic data paired with natural language. To further  
191 improve C2S-Scale's question answering capabilities, we employ Reinforcement Learning (RL) [43] through Group  
192 Relative Policy Optimization (GRPO) to further optimize the model to generate preferred responses to questions  
193 (Fig. 7B). By using BioBERTScore as the reward function, we guide C2S-Scale toward producing higher-quality  
194 answers aligned with biological insights. Following GRPO training, C2S-Scale significantly outperforms the SFT  
195 baseline on the scQA dataset, highlighting the potential of RL techniques to optimize LLMs for specialized single-cell  
196 applications.

197 **2.7 Perturbation Response Prediction**

198 Single-cell foundation models offer remarkable opportunities for conducting large-scale virtual perturbation experiments  
199 that would otherwise be infeasible or prohibitively expensive in a laboratory setting. Here, we demonstrate C2S-Scale's  
200 generalization capabilities across unseen perturbations and cellular contexts, along with its broad applicability for  
201 modeling perturbation responses (Fig. 8A).

202 Training proceeds in two stages (Figure 8C): supervised fine-tuning (SFT) to predict gene-expression profiles of  
203 untreated cells—including L1000 cell lines—under specified perturbation conditions, followed by online reinforcement  
204 learning with GRPO [35] that optimizes biologically relevant objectives. We designed the reward function to prioritize  
205 the accurate prediction of key gene programs of interest. This includes apoptosis for L1000 [44] and interferon response  
206 for Dong et al. [45]. Concretely, the reward is computed over these targeted gene subsets (Figure 8F), which focuses  
207 optimization while preserving full-profile generation and improves out-of-distribution generalization (Figure 8G).

208 We introduce a new metric, scFID (Fig. 8B), an adaptation of the FID metric [46] widely used in computer vision to  
209 evaluate the realism of generated images. scFID adapts the FID metric by replacing the Inception-v3 model with a  
210 single-cell foundation model to embed transcriptomic data, enabling evaluation of generated cells in a representation  
211 space aligned with biological structure and functional gene programs. By assessing differences in this embedding space  
212 rather than at the level of individual genes, scFID captures higher-order variation across cell states, yielding stable  
213 model rankings (Fig. 8E) and aligning with distributional similarities evident in cell-state embeddings (Fig. 8D), while  
214 complementing expression-level metrics such as Kendall's  $\tau$  and Pearson's  $r$  (Fig. 8G).

215 C2S-Scale outperforms existing methods on the Dong et al. dataset, accurately predicting responses to unseen cytokine  
216 perturbations on entire gene expression profiles. It generalizes to novel combinations of cell type, cytokine, and exposure  
217 duration, highlighting its ability to transfer to completely new contexts not seen during training (Fig. 8E). Compared to  
218 baselines, C2S-Scale performs best on fully unseen combinatorial perturbations, capturing nonlinear synergistic effects.  
219 Quantitative results (Fig. 8F) show superior MMD, Wasserstein, and scFID scores relative to competing models. GRPO  
220 further reduces scFID on interferon-related genes by 16%, thereby improving biological fidelity on immune pathways  
221 (Fig. 8G).

222 The L1000 results further underscore C2S-Scale's versatility in modeling perturbation responses across single-cell  
223 and bulk transcriptomic data. We evaluate performance on apoptosis-related genes, focusing on generalization to  
224 unseen compound treatments. Applying GRPO yields consistent gains (Fig. 8G), improving Kendall's  $\tau$  by 9.2%  
225 for the 410M model and 4.9% for the 1B model, and Pearson's  $r$  by 6.6% for the 410M model and 3.6% for the 1B  
226 model. Rewards are defined on phenotype-linked gene programs (e.g., apoptosis in L1000 [44] and interferon response  
227 [45]; Fig. 8F), which yields context-aware scores well suited for virtual screening and candidate prioritization, while  
228 preserving full-profile prediction and enhancing out-of-distribution generalization (Fig. 8G).

229 **2.8 Immune-context virtual screening reveals a cytokine-conditional amplifier of antigen presentation**

230 A differentiating feature of C2S-Scale is its ability to connect complex transcriptional states across diverse biological  
231 contexts. To test whether C2S-Scale can uncover context-dependent determinants of immune visibility, we programmed  
232 a dual-context in-silico screen that predicts drug effects on MHC-I antigen-presentation programs in immune-context-  
233 positive versus immune-context-neutral cytokine signaling settings. Leveraging its demonstrated strength in perturbation  
234 response prediction, the model identified **silmitasertib**, a CK2 inhibitor, as one of the top candidates with a pronounced  
235 context split: a strong predicted increase in antigen-presentation programs in the immune-context-positive condition of  
236 low-level interferon (IFN) signaling (Fig. 9B; other drugs known to upregulate MHC-I highlighted in blue), but little  
237 to no effect in the neutral condition (Fig. 9C). We selected low-level IFN signaling as a tissue-specific regulator of  
238 immunity that is frequently present, but insufficient to drive maximal antigen presentation. We reasoned that enhanced  
239 antigen presentation in this context has the potential to drive increased T cell recognition, further IFN production, and  
240 positive feedback.

241 Our results were notable because silmitasertib has not been reported in the literature to enhance MHC-I expression,  
242 highlighting the novelty of both the effect itself and its context dependence. We confirmed that interferon response,  
243 quantified by a rank-based score for an interferon-stimulated gene set, was elevated in the immune-context-positive  
244 sample, but negligible in the neutral sample (Fig. 9D). Based on both the model's predictions and the known role  
245 of interferons in MHC-I regulation, we hypothesized that the compound acts as an interferon-conditional amplifier,  
246 lowering the response threshold to interferon rather than initiating antigen presentation de novo (Fig. 9E).

247 We validated this hypothesis in two human neuroendocrine cell models that were completely unseen in C2S-Scale's  
248 training data. In the first model (Merkel cell origin), silmitasertib alone did not alter HLA-A,B,C surface levels, whereas  
249 the combination of low-dose IFN- $\beta$  and silmitasertib produced a marked increase in MHC-I mean fluorescence intensity

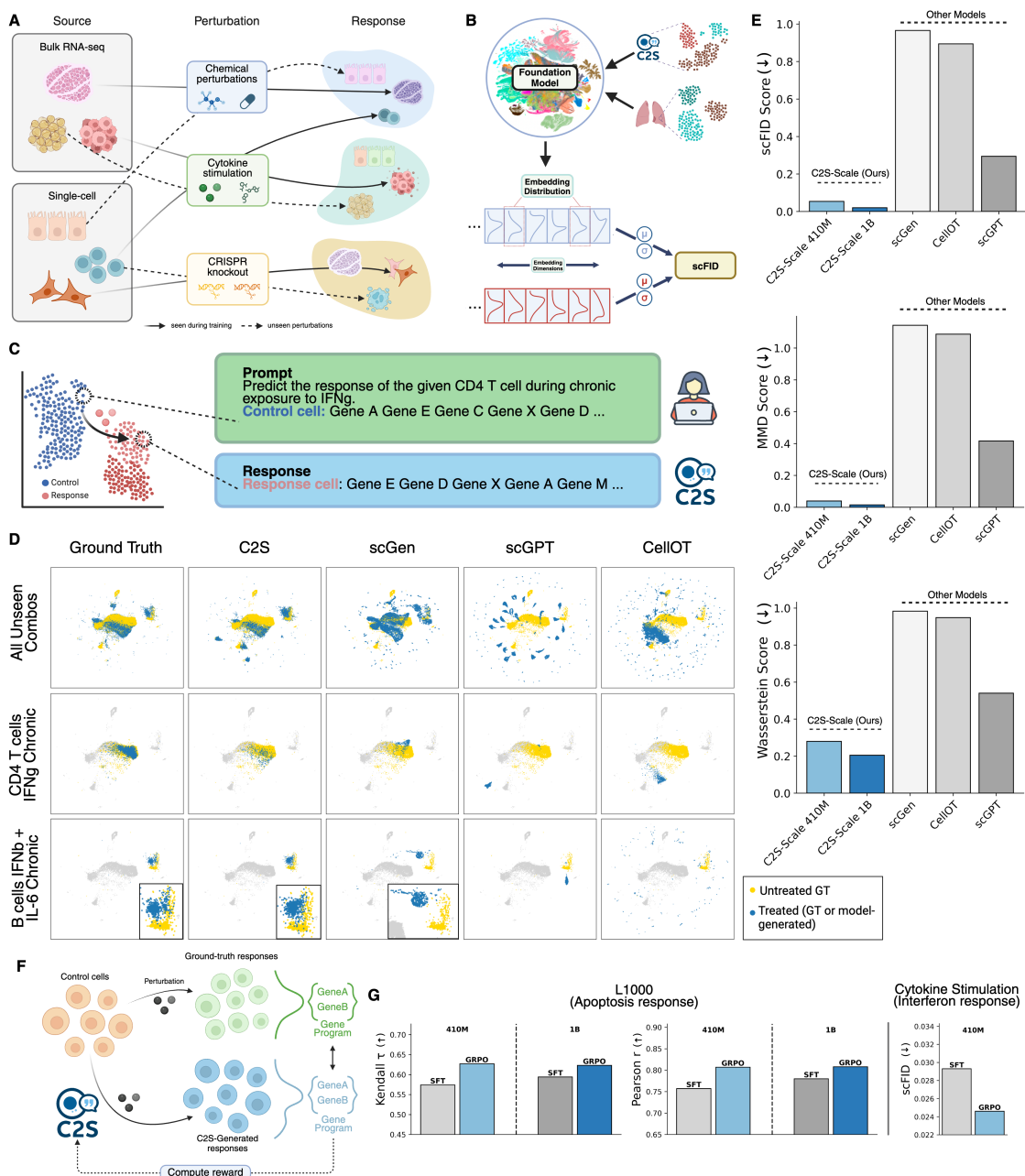


Figure 8: C2S-Scale models outperform existing methods in predicting cellular responses to unseen perturbations. (A) Overview of the C2S-Scale perturbation prediction framework, which supports diverse perturbation types including drugs, cytokines, and genetic knockouts. (B) Diagram of the scFID metric, computed in foundation model latent space, analogous to FID in computer vision. (C) Prompt and response example for perturbation prediction. (D) UMAPs comparing predicted vs. ground-truth responses for unseen perturbations across four models. Rows show: (1) all combinatorial perturbations, (2) CD4 T cells under IFN- $\gamma$ , (3) B cells under the held-out IFN- $\beta$  + IL-6 stimulation. C2S-Scale aligns closely with ground truth in all cases. (E) Benchmark metrics show C2S-Scale outperforms scGen, scGPT, and CellOT across all evaluation criteria. (F) GRPO framework for perturbation prediction: models generate perturbed responses and receive rewards based on gene program similarity. (G) GRPO improves over SFT on L1000 (apoptosis response) and cytokine stimulation (interferon response) tasks, with gains in Kendall's  $\tau$ , Pearson's  $r$ , and scFID.

250 (MFI) (Fig. 9F; 13.6% increase MHC-I MFI at 10nM and 34.9% at 1000nM). The amplification effect generalized  
251 across interferon subtypes (IFN- $\gamma$ , Fig. 9G; 24.9% increase MHC-I MFI at 10nM and 37.3% at 300nM) and was  
252 reproduced in a second, independent human cell model (pulmonary origin, Fig. 9H; 17.1% increase MHC-I MFI at  
253 10nM and 28.1% at 100nM). Notably, neuroendocrine cells were minimally represented in the training data for our  
254 model, with no representation of Merkel cells at all.

255 This discovery of a novel cytokine-conditional amplifier of antigen presentation demonstrates C2S's ability to perform  
256 high-throughput virtual screens to identify promising therapeutic candidates to validate experimentally. Additionally, it  
257 illustrates how C2S can reveal context-conditioned biology that is missed in context-neutral assays.

### 258 3 Discussion

259 Although artificial intelligence approaches including neural network models have achieved significant breakthroughs in  
260 protein structure and the prediction of molecular interactions, less progress in modeling multi-cellular tissues, pathologic  
261 states, and context-specific biology has been made. Principal challenges in this space include the underlying diversity,  
262 complexity, and pleiotropy of biological systems, which compounds across hierarchical organization from genes to  
263 transcriptional programs, and cells to tissues to organisms. Indeed, the semantic complexity and contextuality of  
264 biological systems seems unrivaled—outside of language itself. Our work introduces C2S-Scale, a family of LLMs for  
265 single-cell analysis that leverages the benefits of state-of-the-art LLMs out of the box. By converting transcriptomic  
266 profiles into “cell sentences,” C2S-Scale avoids the need for bespoke model architectures while readily integrating  
267 contextual information from annotations, metadata, and biological texts. This data engineering paradigm yields a  
268 flexible system capable of predictive and generative single-cell tasks, and our results demonstrate that scaling C2S-Scale  
269 up to 27 billion parameters systematically boosts performance, mirroring similar scaling phenomena observed in the  
270 broader field of NLP.

271 Moreover, we show that C2S-Scale bridges the gap between raw transcriptomic information and natural language-  
272 based interpretation by supporting tasks at multiple scales, ranging from cell type annotation to entire dataset-level  
273 summarization. We propose new evaluation datasets for these interpretation tasks and demonstrate that LLMs trained in  
274 the C2S-Scale framework provide meaningful captions and summarizations of single-cell data, even in cases where  
275 the dataset is completely new to the model. By aligning expression data with rich textual metadata and biological  
276 domain knowledge, our approach highlights the potential of language-based modeling to offer biologically informed  
277 explanations and generate insights unavailable to purely expression-only systems.

278 Context-specific decoding is a core task for both LLMs and biological systems alike. To test the ability of C2S-Scale  
279 to derive context-specific biological meaning, we conducted a conditional virtual screen, identifying an IFN-specific  
280 regulator of antigen presentation. We validated the effectiveness of silmitasertib in neuroendocrine Merkel cell and  
281 pulmonary cell models in which the downregulation of antigen presentation machinery is a well-established mechanism  
282 of resistance to immunotherapies. This success provides a blueprint for future screens targeting other complex biological  
283 contexts.

284 We anticipate that higher-capacity models and more diverse training corpora will unlock advanced capabilities, such  
285 as the integration of epigenomic, proteomic, and clinical data into a single multimodal model. In parallel, increasing  
286 transparency and explainability in LLM decision making will be essential for building trust and accelerating adoption of  
287 these tools in single-cell research. Reinforcement Learning and other innovations in LLM alignment will provide a path  
288 forward for aligning LLMs to preferred responses in the context of biological tasks. By directly linking natural language  
289 and transcriptomic data, C2S sets the stage for transformative innovations in biological discovery and personalized  
290 medicine.

### 291 4 Methods

292 The following section details the data collection, processing, and formatting for multi-task samples, as well as the model  
293 architecture for Large Language Models.

#### 294 4.1 Data Collection

295 To construct the C2S-Scale pretraining corpus, we assembled over 50 million single-cell transcriptomic profiles from  
296 human and mouse tissues. Datasets were obtained from established public repositories, including the CELLxGENE [2]  
297 and Human Cell Atlas [3] data portals, and span a wide range of tissues, disease states, and experimental conditions.  
298 Each dataset was accompanied by author-provided metadata, such as cell type and tissue annotations, donor information,

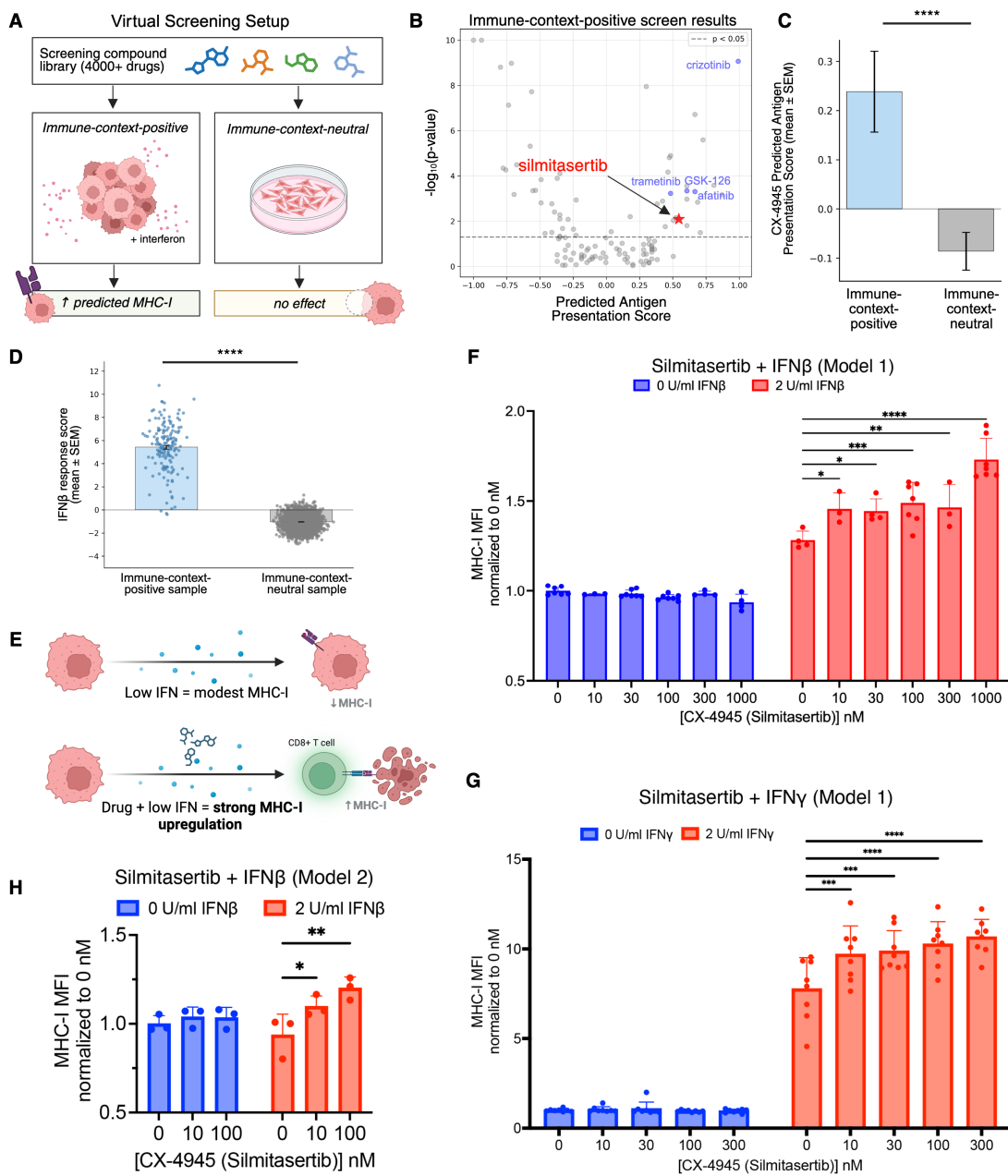


Figure 9: Immune-context virtual screening identifies a cytokine-conditional amplifier of antigen presentation. (A) Schematic of a dual-context virtual screen that predicts drug effects on immune visibility (MHC-I program) in immune-context-positive (primary human samples with endogenous interferon signaling) versus immune-context-neutral (isolated cell) settings. (B) Ranked predictions in the immune-context-positive screen nominate silmitasertib, a CK2 inhibitor, among top candidates to increase antigen-presentation programs (highlighted in red). Selected positive controls known to upregulate MHC-I are highlighted in blue. (C) Silmitasertib shows a context split, with a strong predicted effect in the immune-context-positive setting and negligible effect in the immune-context-neutral setting. (D) Interferon response was quantified by a rank-based score of a curated interferon-stimulated gene set (see Methods). Each point is one sample; bars = mean±SEM; \*\*\*\*,  $P < 0.0001$  (Wilcoxon test). (E) Hypothesis: the compound is an interferon-conditional amplifier that lowers the response threshold for STAT1/IRF1 and thereby amplifies MHC-I upregulation. (F) Experimental validation in an unseen cell type shows no effect of CK2 inhibition alone and marked HLA-A,B,C upregulation in the presence of low-dose IFN- $\beta$  ( $n=3$  independent experiments; points = replicates; bars = mean±SD.; two-sided tests with multiple-comparison correction). (G) The amplification holds with IFN- $\gamma$ , indicating robustness across interferon subtypes. (H) The same interferon-conditional amplification is observed in a second, independent human cell model, supporting generality.

299 developmental stage, and associated study identifiers. Where available, supplementary textual resources, including  
300 paper abstracts and study descriptions, were also retained.

301 Raw scRNA-seq data were processed using standard preprocessing pipelines, including quality control, library size  
302 normalization, and log-transformation, following established conventions [47]. For each dataset, the transcriptomic  
303 profiles were converted into cell sentences, and the accompanying annotations were preserved to construct natural  
304 language prompts. This resulted in a multimodal corpus linking expression profiles with textual descriptors of biological  
305 context. A complete list of datasets included in the corpus is provided in Supplementary Table 1.

#### 306 4.2 Cell Sentence Transformation

307 To adapt high-dimensional single-cell gene expression data into a format compatible with natural language processing,  
308 we converted expression profiles into textual representations termed “cell sentences.” For each cell, let  $X \in \mathbb{R}^D$  be the  
309 expression vector, where  $X_k$  denotes the normalized expression value of gene  $k$  in that cell. The cell sentence for  $X$  is  
310 constructed by rank-ordering the genes within a cell by their expression levels and taking the  $K$  most highly expressed  
311 genes. If  $S$  is a list of indices from 1 to  $D$  sorted in descending order based on expression level in  $X$ , then

$$\text{cell sentence}(X) := \text{"gene}(S[1]) \text{ gene}(S[2]) \dots \text{ gene}(S[K])\text{"}.$$

312 The gene names are in natural language, forming a sentence interpretable by language models (exemplified in Fig. 2).  
313 Under this framework, there is no need to extend or modify the vocabulary of the language model, and it allows any  
314 LLM architecture to tokenize gene names according to their existing vocabulary. This has two primary benefits: (i)  
315 by avoiding architectural modifications, the C2S framework is immediately applicable to any LLM architecture or  
316 innovation, and (ii) the LLM is able to recognize gene names and associate prior knowledge about that gene obtained  
317 during self-supervised pretraining on natural language data, which has been shown to be significant for large-scale  
318 pretrained LLMs [21].

319 The cell sentence transformation into textual sequences retains the underlying biological information by preserving  
320 the rank-order of gene expression. We find there is a strong linear relationship (in log space) between a gene’s rank in  
321 the cell sentence and the (normalized) expression level, validating the fidelity of this transformation. This relationship  
322 is shown in Supplementary Fig. 10 for two scRNA-seq datasets. A linear model fitted between rank and original  
323 expression can predict the original gene expression values given a gene’s rank with  $R^2 = 0.85$ , demonstrating that  
324 minimal information is lost during conversion to cell sentences. This interchangeability allows us to utilize the strength  
325 of LLMs in natural language processing while retaining the ability to convert back to gene expression vectors for  
326 traditional single-cell analysis methods. The parameters of the linear model for each scRNA-seq dataset used during  
327 training are saved to enable reversible transformation from cell sentences back to expression values during inference.

##### 328 4.2.1 Multi-Task Prompt Formatting.

329 C2S-Scale was designed to operate in natural language, enabling a broad range of predictive and generative tasks  
330 in single-cell analysis. These tasks include cell type and tissue annotation, multi-cell generation, and dataset-level  
331 interpretation. The complete list of pretraining tasks, together with their inputs and outputs, is provided in Table 1.

332 Prompts were constructed by combining the cell sentence representation of one or more cells with task-specific natural  
333 language instructions. For predictive tasks, the input prompt included a cell sentence and an instruction, and the output  
334 corresponded to the metadata label of interest. For example, in the cell type annotation task, the input consisted of the  
335 cell sentence and the instruction “Predict the cell type of this cell”, and the output was the corresponding cell type label.  
336 For generative tasks, this structure was inverted: metadata conditions were provided in the input prompt, and the model  
337 was trained to generate one or more cell sentences in response.

338 Metadata included in natural language prompts encompassed cell type, tissue annotations, perturbation conditions,  
339 disease states, and text from associated studies or abstracts, thereby providing additional biological context. This  
340 framework enables C2S-Scale to interpret instructions, integrate biological knowledge, and generalize across diverse  
341 applications.

#### 342 4.3 C2S-Scale architecture and pretraining

##### 343 4.3.1 Input representation

344 C2S-Scale employs large language models (LLMs) based on the Transformer architecture [8] to model cell sentences in  
345 natural language. Input sequences are represented as high-dimensional embeddings suitable for processing by neural  
346 networks. Each word in a cell sentence corresponds to a gene name, which is first tokenized using the pretrained

347 tokenizer associated with the backbone model. This approach avoids the introduction of new vocabulary and maintains  
348 compatibility with the LLM's pretraining knowledge.

349 Tokenized gene names are mapped into vector representations through an embedding layer trained alongside the model.  
350 These embeddings capture semantic properties of genes informed both by their biological context and by the pretrained  
351 model's prior knowledge. Positional encodings are added to preserve the rank order of genes within each cell sentence,  
352 allowing the model to learn dependencies across expression-ranked sequences.

### 353 **4.3.2 Attention mechanism**

354 The central component of the Transformer is the self-attention mechanism [48, 8], which enables the model to compute  
355 pairwise relationships between tokens. For single-cell tasks, this allows the model to dynamically prioritize genes that  
356 are most informative for a given context, such as lineage-defining markers for classification or perturbation-responsive  
357 genes for prediction. The attention mechanism also extends naturally to metadata tokens (e.g. cell type, tissue, disease  
358 state), enabling the model to integrate gene expression with contextual information in a shared representation.

### 359 **4.3.3 Model architecture**

360 C2S-Scale adopts a decoder-only Transformer design [19], chosen for its capacity to model sequential data and support  
361 generative tasks. The architecture consists of a stack of Transformer blocks, each containing a multi-head self-attention  
362 layer followed by a position-wise feedforward network. Residual connections and layer normalization are applied  
363 throughout to stabilize optimization and facilitate scaling to billions of parameters. This modular structure allows the  
364 model to capture long-range dependencies in gene expression data while remaining computationally efficient.

### 365 **4.3.4 Pretraining objective**

366 The model is pretrained with a next-token prediction objective [49], in which the model learns to predict the next  
367 token in a sequence given all preceding tokens. Applied to cell sentences, this involves predicting the next gene in the  
368 rank-ordered expression list, optionally conditioned on metadata tokens. This autoregressive formulation encourages  
369 the model to capture the hierarchical organization of gene expression programs and to integrate biological context  
370 during generation.

371 In contrast to masked-token objectives such as those used in Geneformer [5], which predict randomly masked genes  
372 in non-linguistic sequences, the autoregressive objective aligns naturally with downstream generative applications.  
373 Training the model in this way conditions it to produce coherent, biologically meaningful outputs for tasks such as cell  
374 generation, dataset-level interpretation, and question answering.

### 375 **4.3.5 Training Setup**

376 Pretraining was carried out on the C2S-Scale corpus of more than 50 million single-cell transcriptomes with associated  
377 metadata and textual annotations. A multi-task learning framework was used to jointly optimize across the pretraining  
378 tasks described in Table 1, enabling the model to integrate transcriptomic and contextual information.

379 The C2S-Scale 410M-parameter and 1B-parameter models were trained on one Nvidia A100/H100 GPU with the  
380 Transformers library (version 4.46.3) [50] and PyTorch (version 2.4.1) [51] on a High Performance Computing (HPC)  
381 cluster running Red Hat Enterprise Linux release 8.10. Models larger than 1B parameters were trained on 256 TPU v4s  
382 using the Jax library. We used a starting learning rate of 1e-5 with linear decay and weight decay of 0.01.

## 383 **4.4 Scaling Evaluation**

384 To evaluate scaling behavior in C2S-Scale models, we benchmarked models ranging from 410 million to 27 billion  
385 parameters, based on the Gemma 2 [52] and Pythia [53] architectures. We assessed performance on a held-out set of 500  
386 test samples spanning multiple single-cell tasks listed in Table 1, including cell type annotation, dataset interpretation,  
387 and conditional sample generation tasks. Both fully fine-tuned and LoRA fine-tuned variants [54] were evaluated to  
388 assess scaling behavior under different computational budgets.

389 Performance was measured using BERTScore [22] between generated and reference outputs for predictive tasks such as  
390 cell type annotation and dataset interpretation, providing a semantic measure of response quality. Let the reference  
391 output be  $x = \langle x_1, \dots, x_k \rangle$  and the generated output be  $\hat{x} = \langle \hat{x}_1, \dots, \hat{x}_l \rangle$ , where tokens are represented by contextual  
392 embeddings. Pairwise similarity between tokens is given by the cosine similarity  $s(x_i, \hat{x}_j) = \frac{x_i^\top \hat{x}_j}{\|x_i\| \| \hat{x}_j\|}$ . BERTScore  
393 recall, precision, and F1 are then defined as

Table 1: Pretraining task inputs and outputs for C2S-Scale multi-task training. For multi-cell tasks, multiple cells are sampled from the same donor sample with the same tissue label.

Task name	Type	Input information	Target output	Metric
Single cell language modeling	Single-cell	–	Single cell sentence	Overlap %
Cell type annotation	Single-cell	Single cell sentence	Cell type	BertScore
Conditional cell generation	Single-cell	Cell type of one cell	Single cell sentence	Overlap %
Multiple cell language modeling	Multi-cell	–	Multiple cell sentences	Overlap %
Tissue sample annotation	Multi-cell	Multiple cell sentences	Tissue label	BertScore
Sample cell type(s) annotation	Multi-cell	Multiple cell sentences	Cell types of multiple cells	BertScore
Conditional sample generation (tissue)	Multi-cell	Tissue annotation	Multiple cell sentences	Overlap %
Conditional sample generation (cell type)	Multi-cell	Cell types of multiple cells	Multiple cell sentences	Overlap %
Conditional sample generation (abstract)	Multi-cell	Paper abstract	Multiple cell sentences	Overlap %
Natural language interpretation	Multi-cell	Multiple cell sentences	Paper abstract	BertScore
Gene set enumeration	Gene set	Gene set name	List of genes in gene set	Overlap %
Gene set naming	Gene set	List of genes in gene set	Gene set name	BertScore

$$R_{\text{BERT}} = \frac{1}{|x|} \sum_{x_i \in x} \max_{\hat{x}_j \in \hat{x}} s(x_i, \hat{x}_j), \quad P_{\text{BERT}} = \frac{1}{|\hat{x}|} \sum_{\hat{x}_j \in \hat{x}} \max_{x_i \in x} s(x_i, \hat{x}_j),$$

$$F_{\text{BERT}} = \frac{2 P_{\text{BERT}} R_{\text{BERT}}}{P_{\text{BERT}} + R_{\text{BERT}}}.$$

394 This formulation captures semantic similarity even when exact lexical matches are absent. Unless otherwise noted, all  
 395 reported BERTScore values correspond to the F1 variant.

396 For generative tasks such as conditional cell generation, we evaluated outputs by measuring gene overlap between  
 397 generated and target cell sentences. This metric captures the proportion of ground truth genes recovered in the generated  
 398 output, providing a direct measure of transcriptomic fidelity. Let  $G_{\text{ref}}$  denote the set of genes in the reference cell  
 399 sentence and  $G_{\text{gen}}$  the set of genes in the generated cell sentence. Gene overlap is defined as

$$\text{Overlap}(G_{\text{gen}}, G_{\text{ref}}) = \frac{|G_{\text{gen}} \cap G_{\text{ref}}|}{|G_{\text{ref}}|}.$$

## 400 4.5 Post-training methods

### 401 4.5.1 Supervised fine-tuning

402 C2S-Scale was adapted to downstream applications through supervised fine-tuning on labeled datasets. Fine-tuning  
 403 used the same autoregressive next-token prediction objective as pretraining, with prompts formatted to match each task.  
 404 For example, a prompt might consist of a cell sentence followed by the instruction “Predict the tissue of origin for this  
 405 cell:”, and the model was trained to output the corresponding metadata label.

406 Parameter-efficient strategies were used to limit overfitting and reduce compute cost. Low-Rank Adaptation (LoRA)  
 407 and lightweight adapter layers updated only a small subset of parameters, while the majority of pretrained weights  
 408 remained frozen. This design allowed rapid task-specific adaptation with modest data requirements.

### 409 4.5.2 Reinforcement learning alignment

410 Reinforcement learning (RL) was used to further align model outputs with biological accuracy and interpretability. We  
 411 employed Group Relative Policy Optimization (GRPO), a policy-gradient method that incorporates task-specific reward  
 412 signals directly into parameter updates [43, 35].

413 The supervised fine-tuned model (policy  $\pi_\theta$ ) generated multiple candidate outputs  $o = (o_1, \dots, o_{|o|})$  for each input  
 414 prompt  $q$ . Each token  $o_t$  was assigned probability  $\pi_\theta(o_t | q, o_{<t})$ , where  $o_{<t}$  denotes the prefix. Rewards  $r_i$  were  
 415 assigned to each candidate sequence  $o_i$  using automated evaluation metrics such as BERTScore [22] and domain-specific  
 416 scores for tasks like perturbation response prediction.

417 Proximal Policy Optimization (PPO) maximizes a clipped surrogate objective, which requires estimating per-token  
 418 advantages  $A_t$  using a value function:

$$J_{\text{PPO}}(\theta) = \mathbb{E}_{q \sim P(Q), o \sim \pi_{\theta_{\text{old}}}} \left[ \frac{1}{|o|} \sum_{t=1}^{|o|} \min \left( \frac{\pi_\theta(o_t | q, o_{<t})}{\pi_{\theta_{\text{old}}}(o_t | q, o_{<t})} A_t, \text{clip} \left( \frac{\pi_\theta(o_t | q, o_{<t})}{\pi_{\theta_{\text{old}}}(o_t | q, o_{<t})}, 1 - \epsilon, 1 + \epsilon \right) A_t \right) \right],$$

- 419 where  $\pi_{\theta_{\text{old}}}$  is the policy from the previous iteration,  $A_t$  is the advantage at step  $t$ , and  $\epsilon$  is the clipping threshold.  
 420 Maintaining a critic to estimate  $A_t$  increases computational cost and can destabilize training.  
 421 GRPO replaces the value function with a group-relative baseline. For each prompt  $q$ , the model samples  $G$  candidate  
 422 outputs  $\{o_1, \dots, o_G\}$  with associated rewards  $\{r_1, \dots, r_G\}$ . Relative advantages are defined by normalizing rewards  
 423 across the group:

$$\tilde{r}_i = \frac{r_i - \text{mean}(r)}{\text{std}(r)}, \quad \hat{A}_{i,t} = \tilde{r}_i \quad \forall t \in o_i.$$

- 424 The GRPO objective is

$$J_{\text{GRPO}}(\theta) = \mathbb{E}_{q, \{o_i\}_{i=1}^G} \left[ \frac{1}{G} \sum_{i=1}^G \frac{1}{|o_i|} \sum_{t=1}^{|o_i|} \left( \min \left( \frac{\pi_\theta(o_{i,t} | q, o_{i,<t})}{\pi_{\theta_{\text{old}}}(o_{i,t} | q, o_{i,<t})} \hat{A}_{i,t}, \right. \right. \right. \right. \\ \left. \left. \left. \left. \text{clip} \left( \frac{\pi_\theta(o_{i,t} | q, o_{i,<t})}{\pi_{\theta_{\text{old}}}(o_{i,t} | q, o_{i,<t})}, 1 - \epsilon, 1 + \epsilon \right) \hat{A}_{i,t} \right) - \beta D_{\text{KL}}(\pi_\theta \| \pi_{\text{ref}}) \right) \right] \right],$$

- 425 where  $\pi_{\text{ref}}$  is the frozen SFT model and  $\beta$  controls the KL regularization strength.  
 426 GRPO eliminates the critic network, reduces memory requirements, and yields stable optimization at scale. When  
 427 trained with biologically relevant reward functions, C2S-Scale refined its predictions and aligned generative behavior  
 428 with biological ground truth.

## 429 4.6 Downstream Tasks

### 430 4.6.1 Cell type annotation

- 431 For the cell type annotation task, we fine-tuned the model to predict cell type labels on an immune tissue dataset [55],  
 432 pancreas dataset [56], and a lung dataset [16]. We used 80% of cells from each dataset for training and reserved 20%  
 433 for evaluation. C2S-Scale was provided with a cell sentence and a natural language prompt, such as "Predict the cell  
 434 type of this cell:". C2S-Scale was fine-tuned for this task using the same next-token prediction objective [49] as the  
 435 pretraining step, predicting cell type labels in natural language. Other scFMs were fine-tuned using prediction heads on  
 436 top of the pretrained transformer weights in accordance with the recommended strategies for each model.

### 437 4.6.2 Cell generation

- 438 For cell generation tasks, we fine-tuned the model to unconditionally or conditionally generate cell expression on the  
 439 immune tissue and lung datasets. The model was given a natural language prompt containing relevant metadata for  
 440 conditional generation, or no information in the case of unconditional generation, and was tasked with generating a cell  
 441 sentence of  $K$  genes representing the expression of the cell under that condition. For instance, to conditionally generate  
 442 a B cell, the model might be given a prompt such as: "Generate a list of 1000 genes in order of descending expression  
 443 which represent a Homo sapiens cell of cell type B cell."

### 444 4.6.3 Cell embedding

- 445 For cell embedding, we used C2S-Scale foundation models (e.g. C2S-Scale 1B) trained on the C2S multimodal corpus  
 446 to embed cells without any dataset-specific fine-tuning. To embed cells, we first formatted input prompts for C2S-Scale  
 447 in the same manner as in cell type prediction tasks. However, instead of decoding token predictions, we took the last  
 448 hidden state from the last layer of the C2S-Scale model, and average pooled the latents in order to form our embedding  
 449 of the input prompt. We note that this procedure can be done for multi-cell contexts as well as contexts that involve  
 450 different metadata and condition components in natural language prompts, making C2S-Scale a diverse embedding  
 451 model for transcriptomic and language inputs.

452 **4.6.4 Single-cell bulk integration**

453 Multimodal integration is essential for capturing the complexity of biological systems, as different data modalities  
454 provide complementary perspectives on cellular function. Each modality has its own strengths and limitations: some  
455 offer high resolution at the cost of sparsity, while others provide broader coverage but lack single-cell detail. Therefore,  
456 models that can integrate modalities can provide a more complete and robust understanding of cellular behavior,  
457 improving both interpretability and predictive power in biological analysis.

458 To assess this, we designed a simple single-cell and bulk RNA seq integration task. Using a single-cell lung tissue  
459 dataset [16], we constructed pseudo-bulk samples by aggregating over donor, cell type, and batch. For each pseudo-bulk  
460 sample, we randomly sampled ten single-cell samples from the same conditions to construct pairs. We embedded  
461 each single-cell and pseudo-bulk sample individually using each model and computed the cosine similarity between  
462 the paired single-cell and bulk samples. Following [57], we used the “fraction of samples closer than the true match”  
463 (FOSCTTM) to evaluate the performance of each model. A FOSCTTM of 0 corresponds to a perfect model (the cosine  
464 similarity of matched pairs is higher than any other pair), whereas a FOSCTTM close to 0.5 means the cosine similarity  
465 between the matched pairs is about as good as the cosine similarity between random pairs.

466 **4.6.5 Cluster captioning**

467 To generate the cluster captioning dataset, we selected 30 scRNA-seq datasets and performed standard preprocessing,  
468 clustering, and differential expression analysis. We then prompted GPT-4o [19] to generate five captions for a cluster  
469 based on the cell type, tissue type, organism, disease, top three differentially expressed genes, and the full text of the  
470 associated paper. This resulted in a total dataset of 1,723 captions from 345 distinct clusters. To produce the final  
471 training data, we randomly sampled two cells from a cluster to construct the training prompt, and a caption from that  
472 cluster as the target. The C2S-Scale models were fine-tuned using supervised fine-tuning with a next-token prediction  
473 learning objective with a learning rate of  $1 \times 10^{-5}$ , weight decay of 0.01, and a batch size of 64. All models were  
474 evaluated on the same holdout test set consisting of clusters unseen in the training data.

475 **4.6.6 Dataset interpretation**

476 For the dataset-level interpretation task, we created two test sets for dataset-level interpretation: (i) a training distribution  
477 dataset interpretation test set, where scRNA-seq data and paper abstracts come from 613 of the scRNA-seq datasets  
478 gathered from CELLxGENE [2] as a part of the C2S-Scale training corpus, and (ii) an out-of-distribution (OOD)  
479 evaluation set where the papers and data are completely unseen by the C2S-Scale model. By evaluating dataset-  
480 level interpretation on scRNA-seq studies from both the training corpus and out of distribution data, this serves as a  
481 challenging generalization benchmark for writing meaningful interpretations of scRNA-seq data.

482 Each dataset interpretation sample was created by sampling between 5 and 20 cells from the same tissue and donor in a  
483 given scRNA-seq dataset, and formatting a prompt with the multi-cell context that tasked the model with generating a  
484 biological abstract summary to describe the data. The ground truth for the abstract summary of the data was obtained by  
485 taking the abstract of the paper associated with the scRNA-seq study; to create more diversity in the biological abstracts  
486 seen across samples, we create 500 variations of each dataset abstract using GPT-3.5-Turbo-1106, to prevent the model  
487 from simply memorizing a few hundred dataset abstracts. For each multi-cell context, we choose one of the abstract  
488 summaries as the ground truth target summary. Example abstract summaries can be found in Fig. 11.

489 To create the training corpus distribution dataset interpretation test set, we first gathered held-out abstract generation  
490 samples from the training corpus. These are multi-cell contexts and samples which the model had not seen during  
491 training since they were a part of held-out validation and test sets of the C2S-Scale corpus, however since each dataset  
492 only contains one abstract, the held-out samples will still contain similar information to training set abstract generation  
493 samples that the model has seen. We sampled 5 held-out abstract generation samples from 613 datasets gathered from  
494 CELLxGENE [2], yielding a total test set of 3065 dataset interpretation samples.

495 For the out-of-distribution dataset interpretation test set, we constructed new abstract generation samples by incor-  
496 porating two new datasets from CELLxGENE that were either published recently (after the initial C2S-Scale corpus  
497 gathering period) or verified to not be a part of the C2S-Scale training corpus: (i) a pancreas tissue [56] and a human  
498 retina [58] dataset. We constructed 200 samples from each dataset, again creating 50 variations of the abstract of each  
499 dataset to again provide more diversity in summary language.

500 **4.6.7 Spatial niche prediction**

501 For the spatial niche prediction task, we used the CosMx Spatial Molecular Imager Human Liver dataset [32], which  
502 provides annotated spatially-resolved single-cell data from both normal and hepatocellular carcinoma liver tissues from

503 two different donors. This dataset encompasses over 800,000 single cells across a total of approximately  $180 \text{ mm}^2$  of  
504 liver tissue, with expression measured on a set of 1,000 curated genes. The dataset was processed to filter out genes  
505 expressed in fewer than three cells and cells expressing fewer than 50 genes. It was then normalized to a total count of  
506  $1 \times 10^4$  and the base 10 logarithm was applied. Spatial coordinates were saved to define neighborhoods and facilitate  
507 spatial analyses. We define a neighborhood to be a radius of 0.02 pixels (approximately  $20 \mu\text{m}$ ), chosen to maximize  
508 the number of cells we can fit into the model's context. The dataset was split into training and test sets based on spatial  
509 coordinates to prevent spatial leakage between sets.

510 To train C2S-Scale on spatial and multi-cellular relationships, we designed the following tasks:

- 511 1. **Niche label prediction:** Given a cell sentence for a single cell, predict the niche label annotation for that cell.
- 512 2. **Conditional Neighbor Generation:** Given multiple cell sentences from a neighborhood, generate a novel cell  
513 sentence that would belong to the same neighborhood.
- 514 3. **Spatial neighborhood prediction:** Given multiple cell sentences, predict whether these cells come from the  
515 same neighborhood.
- 516 4. **Same niche prediction:** Given multiple cell sentences, predict whether all of these cells have the same niche  
517 label or different niches.

518 To construct prompts, cell sentences were randomly sampled from the appropriate data split. Multi-cell contexts were  
519 created by taking all cells in the sampled cell's neighborhood for positive samples, or an equivalent number of randomly  
520 sampled cells outside the neighborhood as negative samples. The data contained 19,754 training samples and 3,968 test  
521 samples.

522 Additionally, to enhance the model's understanding of cell communication, we included gene interaction metadata from  
523 CellPhoneDB [33] and BioGRID [34]. We restricted the data to only retain interactions involving the 1,000 genes in the  
524 CosMx data, and also only to genes coding for extracellular proteins (determined using MatrixDB [59]). We included  
525 5,822 interaction samples from CPDB and 2,334 from BioGRID.

526 Models were evaluated on a held-out test set comprising 3,968 samples. Performance was measured as mean prediction  
527 accuracy across the spatial neighborhood prediction tasks. To compare models, paired differences in prediction  
528 outcomes were assessed using McNemar's test with continuity correction, which evaluates whether two classifiers differ  
529 significantly in their error distributions when applied to the same test set. Significance was reported as p-values from  
530 McNemar's test, with values below 0.05 considered statistically significant.

#### 531 4.6.8 Question answering

532 We used the GPT-4.5 model to generate question-answer pairs from three sections of each manuscript (abstracts,  
533 discussions, and results) as well as data sampled from that study. Each scRNA-seq study contributed 20 QA pairs, for a  
534 total of approximately 1600 QA pairs used for SFT. We conduct SFT with a learning rate of  $1 \times 10^{-5}$  and 100 warmup  
535 steps.

536 Following SFT, we applied GRPO to further refine answer quality. To create the GRPO training set, we collected an  
537 additional 600 samples from unseen studies, with each sample prompting the SFT model to generate 32 candidate  
538 answers. We then used BioBERT to compute a reward score for each candidate answer against the ground truth answer  
539 provided by GPT-4.5, capturing its biological plausibility. These BioBERT-derived scores served as the primary reward  
540 signals, guiding the GRPO update step and optimizing model parameters to favor biologically accurate, contextually  
541 relevant responses. For GRPO training, we set  $\beta = 0.03$  and use a learning rate of  $5 \times 10^{-7}$ . Finally, we evaluated the  
542 GRPO-refined model on a new test set derived from unseen studies, and compare its performance against a commonly  
543 used LLM, as illustrated in Fig. 7.

#### 544 4.6.9 Perturbation prediction

545 The Dong et al. dataset [45] dataset includes immune cells exposed to individual and combinatorial cytokines, with  
546 each cell annotated by type, stimulation, and exposure length – yielding 133 conditions. We retained the 5000 most  
547 highly variable genes and evaluated models in the scGPT embedding space [4] using maximum mean discrepancy  
548 (MMD), Wasserstein distance, and scFID (Section 4.7). This embedding-based evaluation provides more meaningful  
549 comparisons than expression-level metrics, which can be skewed by a small number of genes with extreme values.

550 The training of C2S models for the Dong et al. dataset followed a structured two-stage process to effectively predict  
551 responses to unseen cytokine stimulations. The test dataset featured three tiers of held-out perturbations with increasing  
552 difficulty: (1) a completely excluded combinatorial perturbation (interferon- $\beta$  + IL-6), (2) one perturbation entirely

553 held out for each cell type across both chronic and acute conditions (B: interferon-III, CD4 T: interferon- $\gamma$ , CD8 T:  
554 interferon- $\alpha$ 2, Dendritic: interferon- $\beta$  (no chronic cells), NK: IL-6), and (3) one perturbation excluded in either chronic  
555 or acute conditions for each cell type while the other condition remained in training (B: acute interferon- $\beta$ , CD4 T:  
556 acute interferon- $\beta$  + interferon- $\gamma$ , CD8 T: chronic TNF- $\alpha$ , NK: chronic interferon-III). In the first stage, the model  
557 was fine-tuned using supervised learning on both cell sentence generation and natural language label prediction, where  
558 it simultaneously predicted all three labels—cell type, perturbation, and exposure—ensuring it learned bidirectional  
559 relationships between conditions and gene expression. This fine-tuning stage was conducted for 3–4 epochs using the  
560 Hugging Face Trainer on a single H100 GPU.

561 The second stage employed GRPO to refine perturbation response generation. For the Dong et al. dataset, the reward  
562 was computed as the negative mean squared error between generated and ground truth cells, randomly paired under the  
563 same condition labels and embedded using scGPT. GRPO training used 32 generated responses and 32 real cells per  
564 prompt, and was conducted on 4 H100 GPUs for 3 epochs. The interferon subset used for GRPO was defined as the  
565 union of the MSigDB [60] interferon- $\alpha$  and interferon- $\gamma$  hallmark gene sets, intersected with the highly variable genes  
566 (HVGs) from the dataset, resulting in 95 genes.

567 To benchmark against other perturbation response models, we included scGen, CellOT, and scGPT. For scGen, we  
568 used the pertpy library [61] to generate perturbation predictions. For CellOT, we followed the standard procedure  
569 but replaced the encoder with the pretrained encoder from scGen. For scGPT, we added linear encoders for cell type,  
570 perturbation, and exposure, projecting binary vectors into dense vectors, and then added these embeddings to each gene  
571 token embedding before forwarding them through the model.

572 For the L1000 dataset [44], we trained on the 978 landmark genes following quantile normalization. We paired untreated  
573 and treated samples by matching the cell line name. To evaluate generalization, we selected 50 perturbations with fewer  
574 than 1,000 total samples and held out half the cell lines in each perturbation as test data. We used Kendall’s  $\tau$  as the  
575 reward function during reinforcement learning, as it properly accounts for tied ranks. This is especially important for  
576 L1000 where non-expressed genes share the same lowest rank. SFT was conducted using a batch size of 2 and gradient  
577 accumulation of 32, with a learning rate of 1e-4. Training ran on a single H100 GPU for 3,500 steps (approximately  
578 one epoch, though not all data is seen due to dataset size). For GRPO, the model was trained with a batch size of 8 and  
579 gradient accumulation of 4. We generated 24 responses per prompt. The learning rate was set to 1e-6 with a beta value  
580 of 5e-3. Training was distributed across 4 H100 GPUs—three for model training and one for vLLM-based response  
581 generation. GRPO ran for approximately 3,000 steps over 3 epochs, although as with SFT, the model likely saw less  
582 than a full epoch due to data scale.

583 For evaluation, we computed metrics differently across datasets. For the Dong et al. [45] dataset, we computed  
584 maximum mean discrepancy (MMD), Wasserstein distance, and scFID for each unique combination of condition labels  
585 (cell type, cytokine, and exposure duration), and averaged these values across all combinations to obtain the final metric.  
586 For the L1000 dataset [44], we computed Pearson’s  $r$  against the Level 3 gene expression values and Kendall’s  $\tau$  on the  
587 ranks of the gene expression values for each test sample individually and then reported the average across all samples.

588 Kendall’s  $\tau$  measures rank correlation between two ordered lists. Given  $n$  genes, we consider all  $\frac{1}{2}n(n - 1)$  possible  
589 gene pairs. For any pair of genes  $(i, j)$ , if their relative order (which gene is ranked higher) is the same in both the  
590 generated output and the ground-truth ranking, the pair is *concordant*; if their relative order is reversed, the pair is  
591 *discordant*. Tied pairs (where the genes share the same rank in either list) are handled by assigning them the same value.  
592 Kendall’s  $\tau$  is then defined as

$$\tau = \frac{n_c - n_d}{\frac{1}{2}n(n - 1)},$$

593 where  $n_c$  and  $n_d$  denote the number of concordant and discordant pairs, respectively. In our application, the ranks of the  
594 978 L1000 landmark genes are derived from the generated output of the model, where the cell sentence places genes  
595 in descending expression order (e.g., GeneT GeneA GeneS GeneW ...). Genes not present in the model’s output are  
596 assumed to share the lowest possible rank (e.g., if 950 genes are generated, the remaining 28 share rank 951). The same  
597 ranking convention is applied to the L1000 ground-truth sample, where unexpressed genes also share the last rank.  
598 Kendall’s  $\tau$  is then computed between these two ranked lists, yielding a rank-based correlation that is robust to tied  
599 ranks and sparse expression. Only the apoptosis genes from the MSigDB hallmark set that were present in the L1000  
600 landmark gene list were used during GRPO, totaling 40 genes.

## 601 4.7 Single-Cell Fréchet Inception Distance

602 The scFID is an adaptation of the FID [46] tailored for evaluating generative models in single-cell transcriptomics.  
603 While the traditional FID employs the Inception v3 model [62] to extract features from images, scFID utilizes scGPT  
604 [4] as its foundation model to embed single-cell gene expression profiles. Notably, scFID is flexible and can incorporate

any suitable foundation model for embedding. The scFID quantifies the similarity between the distributions of real and generated single-cell embeddings by assuming that these distributions are multivariate normal (Gaussian). Under this assumption, the scFID computes the Wasserstein distance between the two Gaussian distributions, providing a measure of how closely the generated data resembles the real data in the embedding space.

Mathematically, given two sets of single-cell embeddings—one from real cells and one from generated cells—scFID is defined as:

$$\text{scFID} = \|\mu_r - \mu_g\|_2^2 + \text{tr} \left( \Sigma_r + \Sigma_g - 2(\Sigma_r \Sigma_g)^{\frac{1}{2}} \right)$$

where:

- $\mu_r$  and  $\mu_g$  are the mean vectors of the real and generated cell embeddings, respectively,
- $\Sigma_r$  and  $\Sigma_g$  are the covariance matrices of the real and generated cell embeddings, respectively,
- tr denotes the trace of a matrix.

To evaluate generative model performance across various conditions, we computed the scFID for each unique combination of test labels—such as specific cell types, perturbations, and exposure durations—and then averaged these individual scFID values.

#### 4.8 Virtual Screen Setup

**Datasets** We analyzed drug responses in both primary tumor samples and an immortalized cell line in order to capture effects across distinct immune environments. The immune-context-positive data comprised bulk RNA-seq from a pan-cancer atlas [63], which includes 364 tumor specimens spanning 12 cancer types. Cells were sorted by flow cytometry, and we restricted our analysis to the “tumor” compartment, yielding 162 bulk samples. As an immune-context-neutral system, we used the Merkel cell WAGA cell line, as it was not part of the training data for the model. We obtained data from GEO [64], containing 4,199 cells. For the single-cell data, standard preprocessing was applied, including removal of genes expressed in fewer than three cells, removal of cells with fewer than 50 counts, normalization to a total count of  $10^4$  per cell, and log1p transformation.

To quantify type I interferon activity across bulk tumour samples and single cells, we computed a rank-based analytical z-score for a curated interferon-stimulated gene (ISG) set. For each expression profile, all detected genes were ranked by expression level. The mean rank of the ISG set was then compared to the null expectation of randomly distributed ranks using a two-sample Wilcoxon test.

**Compound library** The screening library was derived from the L1000 resource, which catalogs over 30,000 small molecules. Because our goal was to prioritize compounds that could feasibly be validated, we filtered this set using GPT-o3 to predict commercial availability. This step produced a working library of 4,266 drugs.

**Perturbation inference** Drug perturbations were simulated using our C2S-Scale perturbation response prediction model. Each bulk tumor sample was perturbed *in silico* with every drug in the library three times, for a total of  $N = 486$  samples per drug. For the WAGA cell line, 20 representative cells were each perturbed 20 times with every drug for a total of  $N = 400$  samples per drug. Replicates corresponded to independent forward passes through the model, with stochastic sampling at a temperature of 0.3 to introduce variability across predictions.

**Scoring of antigen-presentation programs** Antigen-presentation activity was quantified by calculating enrichment scores for each perturbed profile. We applied single-sample gene set enrichment analysis (ssGSEA) with the “Class I MHC mediated antigen processing and presentation” gene set from MSigDB [60], using the Python package gseapy (v1.1.8) with parameters `sample_norm_method='rank'` and `weight=0`. Scores were aggregated across replicates for each drug and normalized to the interval  $[-1, 1]$ . As a complementary metric, we also computed the average log-fold change for HLA-A,B,C, which produced results consistent with ssGSEA (Supplementary Fig. 12).

Top-ranked drugs were examined for prior evidence of involvement in antigen-presentation pathways. Manual inspection was used to flag compounds not previously reported in the literature, and these were prioritized for further analysis.

#### 4.9 Experimental Validation of Interferon-Conditional Effects

To validate the interferon-conditional effects predicted *in silico*, we performed experiments in two tumor-derived cell lines: MDK-knockout WAGA (Merkel cell carcinoma, MCC) and DMS153 (small cell lung cancer, SCLC). Cells (600,000–2,500,000 cells/ml) were treated with Silmitasertib at the indicated concentrations for 24 hours, followed by

651 stimulation with 2 U/ml human IFN $\beta$  (PBL Assay Science, cat. #11415) or 2 U/ml human IFN $\gamma$  (PBL Assay Science,  
652 cat. #11500) for an additional 24 hours. In parallel, dose–response assays were performed by titrating IFN $\beta$  across a  
653 range of 0.5–200 U/ml to characterize sensitivity to interferon signaling.

654 After treatment, cells were harvested and stained for surface expression of major histocompatibility complex class I  
655 molecules HLA-A,B,C (clone W6/32, BioLegend). Live tumor cells were gated using Zombie Aqua fixable viability  
656 dye (BioLegend) to exclude dead cells prior to analysis by flow cytometry using the CytoFLEX S running CytExpert 2.4  
657 (all Beckman Coulter). All assays were performed in three independent biological replicates. For statistical comparisons,  
658 a two-way Brown–Forsythe and Welch ANOVA was applied, followed by Dunnett’s T3 correction for multiple testing.

#### 659 **4.10 Data Availability**

660 A list of HCA and CELLxGENE datasets used for pretraining is provided in Supplementary Table 1. Spatial transcriptomic  
661 data for the niche prediction task was obtained from CosMx [32]. Publicly available interaction databases were  
662 acquired from [33, 34, 59]. For the perturbation prediction task we used transcriptomic data from L1000 [44] and from  
663 [45]. For the virtual screen we used primary tumor data from [63] and cell line data from [64]. Model weights are  
664 available on Hugging Face.

#### 665 **4.11 Code Availability**

666 Code for model training is publicly available at: <https://github.com/vandijklab/cell2sentence>

### 667 **5 Acknowledgements**

668 The authors thank collaborators and contributors from across institutions for their invaluable support and insights through-  
669 out this project. This work was supported in part by the National Institutes of Health (NIH) grant R35GM143072–01  
670 and the Yale Colton Center Award, both awarded to Dr. David van Dijk.

671 All figures were created in BioRender, <https://BioRender.com>.

### 672 **6 Author Contributions**

673 Project lead: S.A. Rizvi. Model training was done by D.L., A.P., S.Z., E.W., and B.P. Scaling evaluations were done by  
674 S.A.R., and benchmarking across predictive and generative single-cell tasks was done by S.A.R. and A.P. Perturbation  
675 prediction evaluations and scFID implementation were done by D.L. Question answering evaluations were done by S.Z.,  
676 and wet-lab validation experiments were done by C.J.P. and N.M.C. Data curation was done by S.H., D.Z., Z.L., C.L.,  
677 E.S., D.J., and L.Z. Reviewing and editing was done with guidance from C.T., J.K., D.B., B.H., R.D., H.C., R.M.D.,  
678 B.P., J.I., S.Z., and D.v.D. All of the authors reviewed the manuscript.

## 679 References

- 680 [1] Philipp Angerer, Lukas Simon, Sophie Tritschler, F Alexander Wolf, David Fischer, and Fabian J Theis. Single  
681 cells make big data: new challenges and opportunities in transcriptomics. *Current opinion in systems biology*,  
682 4:85–91, 2017.
- 683 [2] CZI Cell Science Program, Shiblea Abdulla, Brian Aevermann, Pedro Assis, Seve Badajoz, Sidney M Bell,  
684 Emanuele Bezzi, Batuhan Cakir, Jim Chaffer, Signe Chambers, et al. Cz cellxgene discover: A single-cell data  
685 platform for scalable exploration, analysis and modeling of aggregated data. *Nucleic Acids Research*, page  
686 gkae1142, 2024.
- 687 [3] Aviv Regev, Sarah A Teichmann, Eric S Lander, Ido Amit, Christophe Benoist, Ewan Birney, Bernd Bodenmiller,  
688 Peter Campbell, Piero Carninci, Menna Clatworthy, et al. The human cell atlas. *elife*, 6:e27041, 2017.
- 689 [4] Haotian Cui, Chloe Wang, Hassaan Maan, Kuan Pang, Fengning Luo, Nan Duan, and Bo Wang. scgpt: toward  
690 building a foundation model for single-cell multi-omics using generative ai. *Nature Methods*, pages 1–11, 2024.
- 691 [5] Christina V Theodoris, Ling Xiao, Anant Chopra, Mark D Chaffin, Zeina R Al Sayed, Matthew C Hill, Helene  
692 Mantineo, Elizabeth M Brydon, Zexian Zeng, X Shirley Liu, et al. Transfer learning enables predictions in  
693 network biology. *Nature*, 618(7965):616–624, 2023.
- 694 [6] Minsheng Hao, Jing Gong, Xin Zeng, Chiming Liu, Yucheng Guo, Xingyi Cheng, Taifeng Wang, Jianzhu Ma,  
695 Xuegong Zhang, and Le Song. Large-scale foundation model on single-cell transcriptomics. *Nature Methods*,  
696 pages 1–11, 2024.
- 697 [7] Ana-Maria Istrate, Donghui Li, and Theofanis Karaletsos. scgenep: Is language all you need for modeling  
698 single-cell perturbations? *bioRxiv*, pages 2024–10, 2024.
- 699 [8] A Vaswani. Attention is all you need. *Advances in Neural Information Processing Systems*, 2017.
- 700 [9] Alec Radford, Jeffrey Wu, Rewon Child, David Luan, Dario Amodei, Ilya Sutskever, et al. Language models are  
701 unsupervised multitask learners. *OpenAI blog*, 1(8):9, 2019.
- 702 [10] Tom Brown, Benjamin Mann, Nick Ryder, Melanie Subbiah, Jared D Kaplan, Prafulla Dhariwal, Arvind Nee-  
703 lakantan, Pranav Shyam, Girish Sastry, Amanda Askell, et al. Language models are few-shot learners. *Advances  
704 in neural information processing systems*, 33:1877–1901, 2020.
- 705 [11] Jared Kaplan, Sam McCandlish, Tom Henighan, Tom B Brown, Benjamin Chess, Rewon Child, Scott Gray,  
706 Alec Radford, Jeffrey Wu, and Dario Amodei. Scaling laws for neural language models. *arXiv preprint  
707 arXiv:2001.08361*, 2020.
- 708 [12] Biao Zhang, Zhongtao Liu, Colin Cherry, and Orhan Firat. When scaling meets llm finetuning: The effect of data,  
709 model and finetuning method. *arXiv preprint arXiv:2402.17193*, 2024.
- 710 [13] Rahul M Dhodapkar. Representing cells as sentences enables natural-language processing for single-cell transcrip-  
711 toomics. *bioRxiv*, pages 2022–09, 2022.
- 712 [14] Daniel Levine, Syed Asad Rizvi, Sacha Lévy, Nazreen Pallikkavaliyaveetil, David Zhang, Xingyu Chen, Sina  
713 Ghadermarzi, Ruiming Wu, Zihe Zheng, Ivan Vrkic, et al. Cell2sentence: Teaching large language models the  
714 language of biology. *bioRxiv*, pages 2023–09, 2023.
- 715 [15] C Domínguez Conde, C Xu, LB Jarvis, DB Rainbow, SB Wells, T Gomes, SK Howlett, O Suchanek, K Polan-  
716 ski, HW King, et al. Cross-tissue immune cell analysis reveals tissue-specific features in humans. *Science*,  
717 376(6594):eabl5197, 2022.
- 718 [16] Jieun Kim, Eun-Young Eo, Bokyong Kim, Heetak Lee, Jihoon Kim, Bon-Kyoung Koo, Hyung-Jun Kim, Sukki  
719 Cho, Jinho Kim, and Young-Jae Cho. Transcriptomic analysis of air–liquid interface culture in human lung  
720 organoids reveals regulators of epithelial differentiation. *Cells*, 13(23):1991, 2024.
- 721 [17] Hugo Touvron, Thibaut Lavril, Gautier Izacard, Xavier Martinet, Marie-Anne Lachaux, Timothée Lacroix,  
722 Baptiste Rozière, Naman Goyal, Eric Hambro, Faisal Azhar, et al. Llama: Open and efficient foundation language  
723 models. *arXiv preprint arXiv:2302.13971*, 2023.
- 724 [18] Hugo Touvron, Louis Martin, Kevin Stone, Peter Albert, Amjad Almahairi, Yasmine Babaei, Nikolay Bashlykov,  
725 Soumya Batra, Prajwal Bhargava, Shruti Bhosale, et al. Llama 2: Open foundation and fine-tuned chat models.  
726 *arXiv preprint arXiv:2307.09288*, 2023.
- 727 [19] Josh Achiam, Steven Adler, Sandhini Agarwal, Lama Ahmad, Ilge Akkaya, Florencia Leoni Aleman, Diogo  
728 Almeida, Janko Altenschmidt, Sam Altman, Shyamal Anadkat, et al. Gpt-4 technical report. *arXiv preprint  
729 arXiv:2303.08774*, 2023.

- 730 [20] Gemini Team, Rohan Anil, Sebastian Borgeaud, Jean-Baptiste Alayrac, Jiahui Yu, Radu Soricut, Johan Schalkwyk,  
731 Andrew M Dai, Anja Hauth, Katie Millican, et al. Gemini: a family of highly capable multimodal models. *arXiv*  
732 preprint arXiv:2312.11805, 2023.
- 733 [21] Yiqun Chen and James Zou. Genept: a simple but effective foundation model for genes and cells built from  
734 chatgpt. *bioRxiv*, pages 2023–10, 2024.
- 735 [22] Tianyi Zhang, Varsha Kishore, Felix Wu, Kilian Q Weinberger, and Yoav Artzi. Bertscore: Evaluating text  
736 generation with bert. *arXiv preprint arXiv:1904.09675*, 2019.
- 737 [23] Abhimanyu Dubey, Abhinav Jauhri, Abhinav Pandey, Abhishek Kadian, Ahmad Al-Dahle, Aiesha Letman,  
738 Akhil Mathur, Alan Schelten, Amy Yang, Angela Fan, et al. The llama 3 herd of models. *arXiv preprint*  
739 arXiv:2407.21783, 2024.
- 740 [24] Antoine Bosselut, Zeming Chen, Angelika Romanou, Antoine Bonnet, Alejandro Hernández-Cano, Badr  
741 Alkhamissi, Kyle Matoba, Francesco Salvi, Matteo Pagliardini, Simin Fan, et al. Meditron: Open medical  
742 foundation models adapted for clinical practice. 2024.
- 743 [25] Yanis Labrak, Adrien Bazoge, Emmanuel Morin, Pierre-Antoine Gourraud, Mickael Rouvier, and Richard Dufour.  
744 Biomistral: A collection of open-source pretrained large language models for medical domains. *arXiv preprint*  
745 arXiv:2402.10373, 2024.
- 746 [26] Rohit Arora, Christian Cao, Mehl Kumar, Sarthak Sinha, Ayan Chanda, Reid McNeil, Divya Samuel, Rahul K  
747 Arora, T Wayne Matthews, Shamir Chandarana, et al. Spatial transcriptomics reveals distinct and conserved  
748 tumor core and edge architectures that predict survival and targeted therapy response. *Nature Communications*,  
749 14(1):5029, 2023.
- 750 [27] Mikala Egeblad, Elizabeth S Nakasone, and Zena Werb. Tumors as organs: complex tissues that interface with the  
751 entire organism. *Developmental cell*, 18(6):884–901, 2010.
- 752 [28] Giuliana Mannino, Cristina Russo, Grazia Maugeri, Giuseppe Musumeci, Nunzio Vicario, Daniele Tibullo,  
753 Rosario Giuffrida, Rosalba Parenti, and Debora Lo Furno. Adult stem cell niches for tissue homeostasis. *Journal*  
754 of *Cellular Physiology*, 237(1):239–257, 2022.
- 755 [29] Zixuan Cang and Qing Nie. Inferring spatial and signaling relationships between cells from single cell transcriptomic  
756 data. *Nature communications*, 11(1):2084, 2020.
- 757 [30] Suoqin Jin, Christian F Guerrero-Juarez, Lihua Zhang, Ivan Chang, Raul Ramos, Chen-Hsiang Kuan, Peggy  
758 Myung, Maksim V Plikus, and Qing Nie. Inference and analysis of cell-cell communication using cellchat. *Nature*  
759 *communications*, 12(1):1088, 2021.
- 760 [31] Erick Armengol, Adam Officer, Olivier Harismendy, and Nathan E Lewis. Deciphering cell–cell interactions and  
761 communication from gene expression. *Nature Reviews Genetics*, 22(2):71–88, 2021.
- 762 [32] Shanshan He, Ruchir Bhatt, Brian Birditt, Carl Brown, Emily Brown, Kan Chantranuvatana, Patrick Danaher,  
763 Dwayne Dunaway, Brian Filanoski, Ryan G Garrison, et al. High-plex multiomic analysis in ffpe tissue at  
764 single-cellular and subcellular resolution by spatial molecular imaging. *BioRxiv*, pages 2021–11, 2021.
- 765 [33] Kevin Troulé, Robert Petryszak, Martin Prete, James Cranley, Alicia Harasty, Zewen Kelvin Tuong, Sarah A  
766 Teichmann, Luz Garcia-Alonso, and Roser Vento-Tormo. Cellphonedb v5: inferring cell-cell communication  
767 from single-cell multiomics data. *arXiv preprint arXiv:2311.04567*, 2023.
- 768 [34] Rose Oughtred, Jennifer Rust, Christie Chang, Bobby-Joe Breitkreutz, Chris Stark, Andrew Willem, Lorrie  
769 Boucher, Genie Leung, Nadine Kolas, Frederick Zhang, et al. The biogrid database: A comprehensive biomedical  
770 resource of curated protein, genetic, and chemical interactions. *Protein Science*, 30(1):187–200, 2021.
- 771 [35] Zhihong Shao, Peiyi Wang, Qihao Zhu, Runxin Xu, Junxiao Song, Xiao Bi, Haowei Zhang, Mingchuan Zhang,  
772 YK Li, Y Wu, et al. Deepseekmath: Pushing the limits of mathematical reasoning in open language models. *arXiv*  
773 preprint arXiv:2402.03300, 2024.
- 774 [36] P Rajpurkar. Squad: 100,000+ questions for machine comprehension of text. *arXiv preprint arXiv:1606.05250*,  
775 2016.
- 776 [37] Dan Hendrycks, Collin Burns, Steven Basart, Andy Zou, Mantas Mazeika, Dawn Song, and Jacob Steinhardt.  
777 Measuring massive multitask language understanding. *arXiv preprint arXiv:2009.03300*, 2020.
- 778 [38] Yubo Wang, Xueguang Ma, Ge Zhang, Yuansheng Ni, Abhranil Chandra, Shiguang Guo, Weiming Ren, Aaran  
779 Arulraj, Xuan He, Ziyan Jiang, et al. Mmlu-pro: A more robust and challenging multi-task language understanding  
780 benchmark. *arXiv preprint arXiv:2406.01574*, 2024.

- 781 [39] Wanjun Zhong, Ruixiang Cui, Yiduo Guo, Yaobo Liang, Shuai Lu, Yanlin Wang, Amin Saied, Weizhu Chen,  
782 and Nan Duan. Agieval: A human-centric benchmark for evaluating foundation models. *arXiv preprint*  
783 *arXiv:2304.06364*, 2023.
- 784 [40] Asma Ben Abacha and Dina Demner-Fushman. A question-entailment approach to question answering. *BMC*  
785 *bioinformatics*, 20:1–23, 2019.
- 786 [41] Ankit Pal, Logesh Kumar Umapathi, and Malaikannan Sankarasubbu. Medmcqa: A large-scale multi-subject  
787 multi-choice dataset for medical domain question answering. In *Conference on health, inference, and learning*,  
788 pages 248–260. PMLR, 2022.
- 789 [42] Qiao Jin, Bhuwan Dhingra, Zhengping Liu, William W Cohen, and Xinghua Lu. Pubmedqa: A dataset for  
790 biomedical research question answering. *arXiv preprint arXiv:1909.06146*, 2019.
- 791 [43] Richard S Sutton and Andrew G Barto. *Reinforcement learning: An introduction*. MIT press, 2018.
- 792 [44] Aravind Subramanian, Rajiv Narayan, Steven M Corsello, David D Peck, Ted E Natoli, Xiaodong Lu, Joshua  
793 Gould, John F Davis, Andrew A Tubelli, Jacob K Asiedu, et al. A next generation connectivity map: L1000  
794 platform and the first 1,000,000 profiles. *Cell*, 171(6):1437–1452, 2017.
- 795 [45] Mingze Dong, Bao Wang, Jessica Wei, Antonio H. de O. Fonseca, Curtis J. Perry, Alexander Frey, Feriel Ouerghi,  
796 Ellen F. Foxman, Jeffrey J. Ishizuka, Rahul M. Dhodapkar, and David van Dijk. Causal identification of single-cell  
797 experimental perturbation effects with cinema-ot. *Nature Methods*, 20(11):1769–1779, 2023.
- 798 [46] Martin Heusel, Hubert Ramsauer, Thomas Unterthiner, Bernhard Nessler, and Sepp Hochreiter. Gans trained by a  
799 two time-scale update rule converge to a local nash equilibrium. In *Advances in Neural Information Processing*  
800 *Systems*, volume 30, 2017.
- 801 [47] Ashraful Haque, Jessica Engel, Sarah A Teichmann, and Tasio Lönnberg. A practical guide to single-cell  
802 rna-sequencing for biomedical research and clinical applications. *Genome medicine*, 9:1–12, 2017.
- 803 [48] Dzmitry Bahdanau. Neural machine translation by jointly learning to align and translate. *arXiv preprint*  
804 *arXiv:1409.0473*, 2014.
- 805 [49] Alec Radford. Improving language understanding by generative pre-training. 2018.
- 806 [50] T Wolf. Huggingface’s transformers: State-of-the-art natural language processing. *arXiv preprint*  
807 *arXiv:1910.03771*, 2019.
- 808 [51] Adam Paszke, Sam Gross, Francisco Massa, Adam Lerer, James Bradbury, Gregory Chanan, Trevor Killeen,  
809 Zeming Lin, Natalia Gimelshein, Luca Antiga, et al. Pytorch: An imperative style, high-performance deep  
810 learning library. *Advances in neural information processing systems*, 32, 2019.
- 811 [52] Gemma Team, Morgane Riviere, Shreya Pathak, Pier Giuseppe Sessa, Cassidy Hardin, Surya Bhupatiraju, Léonard  
812 Hussenot, Thomas Mesnard, Bobak Shahriari, Alexandre Ramé, et al. Gemma 2: Improving open language  
813 models at a practical size. *arXiv preprint arXiv:2408.00118*, 2024.
- 814 [53] Stella Biderman, Hailey Schoelkopf, Quentin Gregory Anthony, Herbie Bradley, Kyle O’Brien, Eric Hallahan,  
815 Mohammad Afrah Khan, Shivanshu Purohit, USVSN Sai Prashanth, Edward Raff, et al. Pythia: A suite for  
816 analyzing large language models across training and scaling. In *International Conference on Machine Learning*,  
817 pages 2397–2430. PMLR, 2023.
- 818 [54] Edward J Hu, Yelong Shen, Phillip Wallis, Zeyuan Allen-Zhu, Yuanzhi Li, Shean Wang, Lu Wang, and Weizhu  
819 Chen. Lora: Low-rank adaptation of large language models. *arXiv preprint arXiv:2106.09685*, 2021.
- 820 [55] C Xu, L Jarvis, T Gomes, S Howlett, D Rainbow, O Suchanek, H King, L Mamanova, K Polanski, N Huang, et al.  
821 Cross-tissue immune cell analysis reveals tissue-specific adaptations and clonal architecture in humans. 2021.
- 822 [56] Maayan Baron, Adrian Veres, Samuel L Wolock, Aubrey L Faust, Renaud Gaujoux, Amedeo Vetere, Jennifer Hyoje  
823 Ryu, Bridget K Wagner, Shai S Shen-Orr, Allon M Klein, et al. A single-cell transcriptomic map of the human  
824 and mouse pancreas reveals inter-and intra-cell population structure. *Cell systems*, 3(4):346–360, 2016.
- 825 [57] Zhi-Jie Cao and Ge Gao. Multi-omics single-cell data integration and regulatory inference with graph-linked  
826 embedding. *Nature Biotechnology*, 40(10):1458–1466, 2022.
- 827 [58] Zhen Zuo, Xuesen Cheng, Salma Ferdous, Jianming Shao, Jin Li, Yourong Bao, Jean Li, Jiaxiong Lu, Antonio  
828 Jacobo Lopez, Juliette Wohlschlegel, et al. Single cell dual-omic atlas of the human developing retina. *Nature*  
829 *Communications*, 15(1):6792, 2024.
- 830 [59] Olivier Clerc, Madeline Deniaud, Sylvain D Vallet, Alexandra Naba, Alain Rivet, Serge Perez, Nicolas Thierry-  
831 Mieg, and Sylvie Ricard-Blum. Matrixdb: integration of new data with a focus on glycosaminoglycan interactions.  
832 *Nucleic acids research*, 47(D1):D376–D381, 2019.

- 833 [60] Aravind Subramanian, Pablo Tamayo, Vamsi K Mootha, Sayan Mukherjee, Benjamin L Ebert, Michael A Gillette,  
834 Amanda Paulovich, Scott L Pomeroy, Todd R Golub, Eric S Lander, and Jill P Mesirov. Gene set enrichment  
835 analysis: a knowledge-based approach for interpreting genome-wide expression profiles. *Proc. Natl. Acad. Sci. U.*  
836 *S. A.*, 102(43):15545–15550, October 2005.
- 837 [61] L Heumos, Yuge Ji, Lilly May, Tessa D Green, Xinyue Zhang, Xichen Wu, Johannes Ostner, Stefan Peidli, Antonia  
838 Schumacher, Karin Hrovatin, M F Mueller, F Chong, Gregor Sturm, Alejandro Tejada, Emma Dann, Mingze  
839 Dong, Mojtaba Bahrami, Ilan Gold, Sergei Rybakov, Altana Namsaraeva, A Moinfar, Zihe Zheng, Eljas Roellin,  
840 Isra Mekki, C Sander, M Lotfollahi, Herbert B Schiller, and Fabian J Theis. Pertpy: an end-to-end framework for  
841 perturbation analysis. *bioRxiv*, August 2024.
- 842 [62] Christian Szegedy, Vincent Vanhoucke, Sergey Ioffe, Jon Shlens, and Zbigniew Wojna. Rethinking the inception  
843 architecture for computer vision. In *Proceedings of the IEEE Conference on Computer Vision and Pattern*  
844 *Recognition (CVPR)*, June 2016.
- 845 [63] Alexis J Combes, Bushra Samad, Jessica Tsui, Nayvin W Chew, Peter Yan, Gabriella C Reeder, Divyashree  
846 Kushnoor, Alan Shen, Brittany Davidson, Andrea J Barczak, et al. Discovering dominant tumor immune archetypes  
847 in a pan-cancer census. *Cell*, 185(1):184–203, 2022.
- 848 [64] K. Fan, J. Becker, and J. Gravemeyer. Waga single cell rna sequencing. Gene Expression Omnibus, NCBI, GEO  
849 Accession: GSE130346, 2019. Homo sapiens, Expression profiling by high throughput sequencing. BioProject:  
850 PRJNA535920. Accessed: 2025-08-14.
- 851 [65] Alexey Dosovitskiy. An image is worth 16x16 words: Transformers for image recognition at scale. *arXiv preprint*  
852 *arXiv:2010.11929*, 2020.
- 853 [66] Daya Guo, Dejian Yang, Haowei Zhang, Junxiao Song, Ruoyu Zhang, Runxin Xu, Qihao Zhu, Shirong Ma, Peiyi  
854 Wang, Xiao Bi, et al. Deepseek-r1: Incentivizing reasoning capability in llms via reinforcement learning. *arXiv*  
855 *preprint arXiv:2501.12948*, 2025.
- 856 [67] Xuezhi Wang, Jason Wei, Dale Schuurmans, Quoc Le, Ed Chi, Sharan Narang, Aakanksha Chowdhery, and Denny  
857 Zhou. Self-consistency improves chain of thought reasoning in language models. *arXiv preprint arXiv:2203.11171*,  
858 2022.
- 859 [68] Niels Mündler, Jingxuan He, Slobodan Jenko, and Martin Vechev. Self-contradictory hallucinations of large  
860 language models: Evaluation, detection and mitigation. *arXiv preprint arXiv:2305.15852*, 2023.
- 861 [69] Cara Su-Yi Leong and Tal Linzen. Language models can learn exceptions to syntactic rules. *arXiv preprint*  
862 *arXiv:2306.05969*, 2023.
- 863 [70] Michael Wilson, Jackson Petty, and Robert Frank. How abstract is linguistic generalization in large language  
864 models? experiments with argument structure. *Transactions of the Association for Computational Linguistics*,  
865 11:1377–1395, 2023.

## 866 7 Supplementary

### 867 7.1 Limitations

#### 868 7.1.1 Addressing Limitations of Causal Attention in Gene Expression Modeling

869 While our approach demonstrates strong empirical performance in modeling single-cell gene expression using autoregressive language models, we acknowledge that causal attention's inherent unidirectionality—favoring high-to-low  
870 gene expression dependencies—could theoretically limit the modeling of true causal biological interactions that flow  
871 from low- to high-expression genes. However, we contend that this constraint does not significantly impede our  
872 objectives and can be mitigated through several complementary strategies. First, our approach aligns with successful  
873 paradigms from vision-language models, where arbitrary tokenization orders paired with causal attention still achieve  
874 state-of-the-art performance [65]. Similar to hybrid vision architectures that combine causal and non-causal attention  
875 layers, our framework could incorporate indirect bidirectional context through auxiliary reasoning tokens or non-causal  
876 gene interactions.

878 **Multi-cell context and reasoning as a corrective mechanism** The model's reasoning capabilities provide additional  
879 corrective potential. Emerging evidence from language modeling demonstrates that explicit reasoning steps can  
880 compensate for causal attention limitations [66, 67, 68]. In our context, intermediate tokens representing biological  
881 pathways or gene interactions enable iterative prediction refinement, effectively circumventing strict unidirectionality.  
882 Furthermore, our multi-cell training framework enables implicit bidirectionality—low-expression genes in one cell can  
883 influence high-expression genes in the following cell, approximating bidirectional attention across a multi-cell context.

884 **Correlation, not causation** It is important to emphasize that our model is designed to capture predictive correlations  
885 over inferring causal gene relationships. This mirrors natural language processing, where autoregressive models  
886 successfully capture statistical correlations despite occasional misalignment between word order and true causal  
887 relationships (e.g. passive constructions) [69, 70]. Our results confirm that expression correlations provide sufficient  
888 predictive power for key biological analysis tasks.

889 **Architectural enhancements** Looking forward, we propose three architectural enhancements to further mitigate  
890 this limitation: (1) bidirectional attention by partitioning gene sequences, (2) variable gene ordering during training  
891 to induce order invariance, and (3) hybrid attention architectures blending causal and non-causal attention layers.  
892 While our current approach already demonstrates that sequential modeling of gene expression—despite lacking natural  
893 ordering—leverages pretrained LLMs without requiring custom architectures, these enhancements aim to further  
894 improve biological fidelity and predictive power.

895 In summary, while causal attention restricts bidirectionality within individual cells, its ability to capture correlations  
896 aligns with our predictive objectives. The combined effects of multi-cell context, reasoning mechanisms, and prospective  
897 architectural improvements position this approach as a robust foundation for single-cell analysis, with multiple pathways  
898 available for extending its biological fidelity.

#### 899 7.1.2 Hallucination and Interpretability

900 A known challenge with large language models is their tendency to generate plausible but incorrect outputs, often  
901 referred to as hallucinations. While our benchmarking focuses on structured biological tasks with ground-truth labels,  
902 more open-ended interpretation tasks—such as abstract generation or cluster captioning—may be susceptible to such  
903 errors. Developing domain-specific safeguards, such as biological fact-checking mechanisms or constrained decoding  
904 strategies, remains an important direction for improving interpretability and reliability in high-stakes settings.

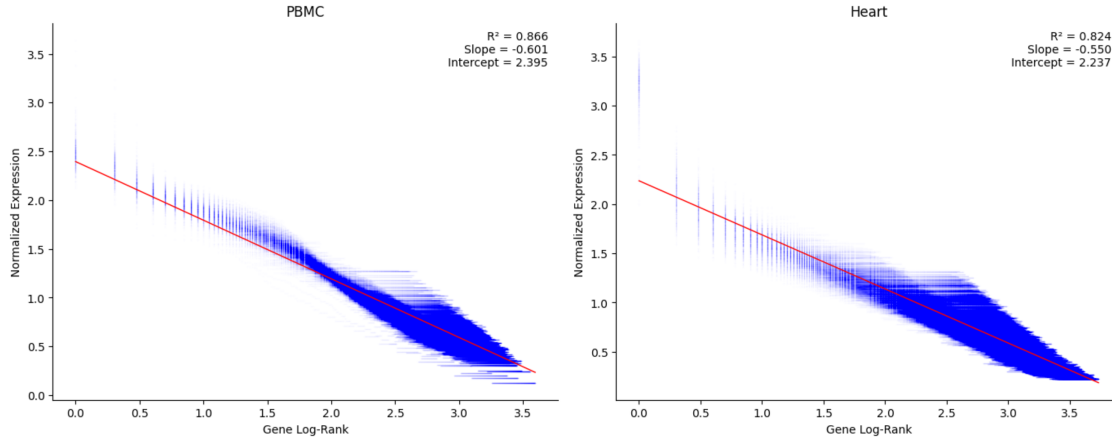


Figure 10: C2S allows for conversion from expression information into cell sentence format with minimal information loss. Using a linear model fitted between rank and original expression, cell sentences can be converted back to expression accurately.

High-throughput single-nucleus RNA sequencing of over three million nuclei from the entire adult human brain identified 461 clusters and 3313 subclusters. The analysis revealed area-specific cortical neurons, diverse midbrain and hindbrain neurons, and regional diversity in astrocytes and oligodendrocyte precursors. This study provides a comprehensive understanding of the molecular diversity of the human brain, offering insights into brain health and diseases.

Single-cell and single-nucleus assays were used to create a detailed atlas of healthy and diseased kidney cells, identifying rare populations and altered cellular states in kidney injury. This revealed biological pathways related to chronic kidney disease progression. The atlas, developed through collaborative efforts, aims to provide a valuable resource for kidney research.

Single-cell RNA sequencing of glioblastoma cells from four patients revealed genomic and transcriptomic variations within the tumor. Infiltrating neoplastic cells shared a consistent gene signature across patients, suggesting a common infiltration mechanism. Additionally, distinct myeloid cell populations were identified in the tumor core and surrounding peritumoral space. This study provides detailed insights into GBM cell types, shedding light on tumor formation and migration.

Figure 11: Example abstract summaries from scRNA-seq datasets collected from CELLxGENE [2].

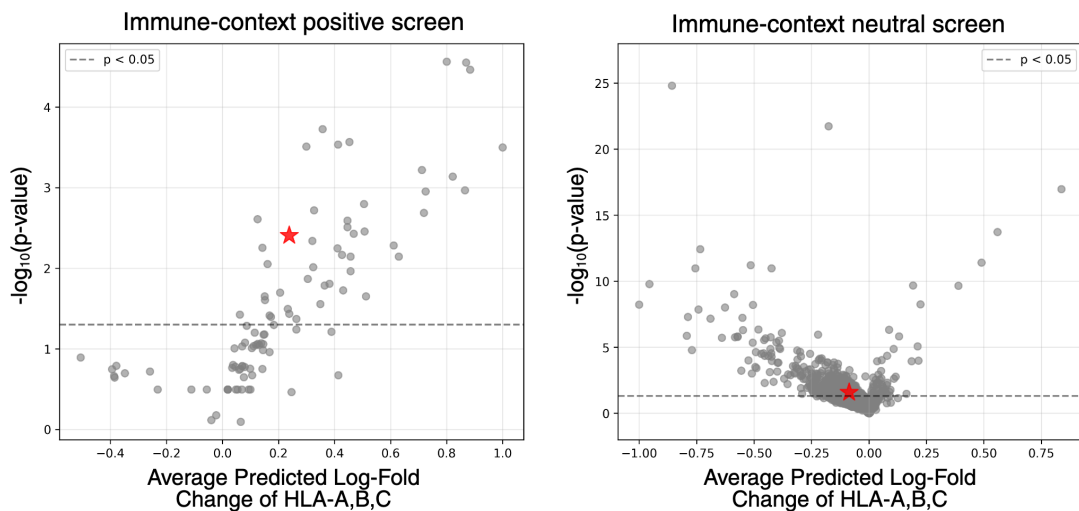


Figure 12: Predicted effects of silmitasertib on MHC-I antigen presentation in immune-context-positive (left) and immune-context-neutral (right) screens. Each point represents a compound, plotted by the average predicted log-fold change of HLA-A,B,C versus the corresponding significance level. Silmitasertib is highlighted in red. Results are consistent with the primary scoring approach using the antigen-presentation gene set (see Methods).